# The temperature-dependent shear strength of ice-filled joints in rock mass considering the effect of joint roughness, opening and shear rates

Shibing Huang[1,2], Haowei Cai[1], Zekun Xin[1], Gang Liu[1]

[1] School of Resources and Environmental Engineering, Wuhan University of Science and Technology, Wuhan, Hubei 430081, China

[2] Hubei Key Laboratory for Efficient Utilization and Agglomeration of Metallurgic Mineral Resources, Wuhan University of Science and Technology, Wuhan, Hubei 430081, China

*Correspondence to*: Shibing Huang (huangshibing@wust.edu.cn)

**Abstract.** Global warming causes many rockfall activities of the alpine mountains, especially when ice-filled joints in the rock mass become thawed. The warming and thawing of frozen soils and intact rocks were widely studied in the past several decades, however, the variation of shear strengths of ice-filled joints was not fully understood. In this study, a series of compression-shear experiments were conducted to investigate the shear strength of ice-filled rock joints by considering the effects of joint roughness, temperature, opening, shear rates and normal stress. The joint roughness can improve the shear strength of ice-filled joints. However, the contribution of joint roughness is controlled by some noticeable bulges instead of the JRC index. The shear strength linearly increases with increasing the aggregation of rupture ice area before these noticeable bulges. As the joint opening increases, the effect of joint roughness decreases and the shear strength of ice-filled joints tends to be equal to the shear strength of pure ice. In addition, the shear strength quickly reduces with increasing temperature from

21    -15 °C to -0.5 °C. The shear failure mode changes from shear cracking of joint ice to the shear

22    debonding of ice-rock interface above -1 °C. Increasing shear rate will decrease the shear strength of

23    ice-filled joints because the joint ice displays the brittle failure phenomenon at a high shear rate. The

24    shear strength of ice-filled joints linearly increases with increasing the normal stress. Moreover, it is

25    also proved that the Mohr-coulomb criterion can be used to characterize the shear strength of ice-filled

26    joints under different normal stresses. This research can provide a better understanding of the warming

27    degradation mechanism of ice-filled joints by considering the above important influencing factors.

28    **1 Introduction**

29    With the increase of global temperature and human activities in permafrost areas, many alpine rock

30    masses become more unstable (Gruber and Haeberli, 2007; Allen and Huggle, 2013; Hartmeyer et al.,

31    2020; Legay et al., 2021; Hilger et al., 2021). A large number of rockfalls in permafrost alpine bedrock

32    slopes indicated the exposure of broken ice after shear failure, which could cause serious natural

33    geological disasters (Krautblatter et al., 2021; Walter et al., 2019). For example, the rockfall disaster

34    that happened in Chamoli, Indian Himalaya, in 2021 took more than 200 lives and destroyed two

35    hydropower facilities (Shugar et al., 2021). According to investigation results, this rockfall disaster was

36    caused by the warming and thawing of ice. It is evidenced that a huge frost heaving pressure will be

37    produced to drive the voids and joints propagation and thus cause the instability of joint rock masses

38    during the freezing process (Huang et al., 2022a; 2022b). Fortunately, the bonding strength between ice

39    and joint wall can strengthen the joints themselves after complete freezing (Matsuoka and Murton,

40    2008; Zhang et al., 2020; Shan et al., 2021; Wang et al., 2022). However, if the joint ice was thawed,

41    the rock-ice-rock "sandwich" structure would be debonded and unstable. In addition, the liquid water

42 produced by warming ice could lower the friction between joint surface and thus reduced the stability

43 of joint rock slopes (Zhao et al., 2017). Many field data showed that most of the irreversible fracture

44 displacement and rockfall happened in the warm seasons instead of the cool seasons because the

45 warming and thawing of joint ice could greatly decrease the strength of rock mass containing ice-filled

46 joints (Weber et al., 2018; Etzelmüller et al., 2022). Yang et al. (2019) claimed that the existence of

47 detached ice block could promote the mobility of ice-rock system and thus cause a more serious

48 geological disaster on alpine rock slope. Therefore, the warming degradation of the ice-rock interface

49 and the strength loss of ice-filled joints should be comprehensively studied.

50 In the past decades, the warming degradation of permafrost soils was widely investigated, however,

51 there is little literature reporting the strength loss of rocks containing ice-filled joints. The shear

52 experiment of the ice-rock interface might be first conducted by replacing the rock with concrete in

53 order to make a specific roughness (Davies et al., 2001, 2017). These experiments were conducted at

54 the temperature from -5 to 0 °C. Krautblatter et al. (2012) developed a shear strength model for the

55 ice-filled joints that incorporates the cracking of rock bridges, the friction of rough joint walls, creep of

56 ice and detachment of rock-ice interfaces. Mamot et al. (2018) conducted a systematic study of the

57 shear failure of limestone-ice and mica-rich interfaces at constant strain rates from -10 to -0.5°C, and

58 they found that the normal stress and freezing temperature were two important factors influencing the

59 shear strength. However, the uniform joint surfaces were used without considering the influence of

60 joint roughness. Mamot et al. (2021) further predicted the warming stability of permafrost slopes

61 containing ice-filled joints by using the Universal Distinct Element Code (UDEC). The simulation

62 results verified that the warming temperature close to the melting point might drive the slide of a slope

63     with angle of 50°-62°, and the actual slope angle also depended on the joint orientation. The above

64     research mainly investigated the thawing temperature and normal stress on the shear strength of

65     ice-filled joints. The highest normal stress is about 1.438 MPa (Davies et al., 2001), and the maximum

66     range for the temperature was -10 °C to -0.5 °C (Mamot et al., 2018). However, the freezing depth

67     could exceed 100 m for some alpine caves containing frozen ice (normal stress large than 2 MPa) and

68     the temperature was less than -15 °C as observed in the field (Colucci and Guglielmin, 2019).

69     Therefore, a much wider range of temperature should be considered when investigating the shear

70     characteristics of ice-filled joints.

71     In addition, although some scholars began to pay attention to the mechanical properties of ice-filled

72     joint rock mass, the influence of many important factors on the shear strength of ice-filled joints was

73     not investigated, including the joint roughness, shear rate, normal stress and joint opening. Generally,

74     the natural joints have different roughness and openings (Shen et al., 2020). In this study, a

75     comprehensive shear experiment was performed on the ice-filled joints in sandstones. The main

76     purpose was to reveal the influencing mechanism of freezing temperature, joint roughness, shear rate,

77     joint opening and normal stress on the shear strength of ice-filled joints in rock masses. This research

78     can provide a better understanding of the warming degradation process of the ice-filled joints and the

79     thawing disaster of alpine mountains in cold regions.

80     **2 Materials and methods**

81     **2.1 Collection of sandstones**

82     The red sandstones collected from Yichang city of Hubei province were used in this experiment. This

83     is a typical sedimentary rock and is widely distributed on the surface of the earth. The block samples

84     with approximately equal P-wave (compressional wave) velocities were chosen to make frozen samples

85     containing ice-filled joints. The basic physico-mechanical properties of this red sandstone are given in

86     Table 1.

87     **Table 1.** The basic physico-mechanical properties of the fresh sandstone.

| Density $(\rho)$ (g/cm³) | Porosity $n$ (%) | Primary wave velocity $V_p$ (m/s) | | Shear strength $\tau_{ps}$ (MPa) | | Uniaxial compressive strength UCS (MPa) | |
|---|---|---|---|---|---|---|---|
| | | Dry | Saturated | Dry | Saturated | Dry | Saturated |
| 2.32 | 7.71 | 2992 | 3264 | 7.60 | 3.02 | 79.53 | 30.97 |

88

89     **2.2 Preparation of ice-filled joint rock mass**

90     According to the JRC index proposed by Barton and Choubey (1977), five kinds of roughness were

91     used in this experiment, including No. 2 (2°-4°), No. 4 (6°-8°), No. 6 (10°-12°), No. 8 (14°-16°) and

92     No. 10 (18°-20°), respectively. The frozen samples containing ice-filled joints are made in the

93     laboratory because it is hard to cut or drill them in the fields. The manufacturing process of ice-filled

94     joint rock mass mainly includes the following steps:

95     ①    The original rock blocks were cut into the designed rectangular blocks (100 mm × 100 mm × 50

96     mm) by using a rock cutting machine.

97     ②    These rectangular blocks were used to engrave different rough curves on the surface by using a

98     3D numerical control engraving machine. The roughness can be controlled by implanting the standard

99     JRC curves into the controlling system of this machine. Each frozen rock sample containing an

100     ice-filled joint was assembled by using a pair of rectangular blocks with the same roughness.

101  ③  The rock blocks were heated in a dry oven at 105 ℃ in order to tightly paste the waterproof tape

102  and prevent the escape of joint water during freezing.

103  ④  The joint opening was divided into different specified thicknesses which were controlled by

104  inserting rubber strips, and a piece of waterproof tape was pasted on the surface in order to store water.

105  ⑤  When the waterproof tape was tightly bonded on the rock surface, liquid water should be injected

106  into the artificial joint until no water leaks out. After that, the water-filled joint rock mass was put into

107  a steel mold to freeze in a freezing chamber. The steel mold was used to control the joint opening

108  because the volume of joint water would expand during freezing. Then ice-filled joint samples can be

109  derived after freezing at -20 ℃ for 12 h. The manufacturing procedure and related ice-filled joint

110  samples were shown in Fig. 1.

111  **Table 2.** Ten standard joint profiles (Barton and Choubey, 1977).

| Profile No. | Typical roughness profiles | JRC range |
|---|---|---|
| No. 1 | | 0-2(0.4) |
| No. 2 | | 2-4(2.8) |
| No. 3 | | 4-6(5.8) |
| No. 4 | | 6-8(6.7) |
| No. 5 | | 8-10(9.5) |
| No. 6 | | 10-12(10.8) |
| No. 7 | | 12-14(12.8) |

| No. 8 | | 14-16(14.5) |
| No. 9 | | 16-18(16.7) |
| No. 10 | | 18-20(18.7) |

112

① Cutting and polishing    ② Engraving by standard JRC    ③ Drying at 105 ℃

Ice-filling joints    ⑤ Injecting water and freezing    ④ Sealing joints up
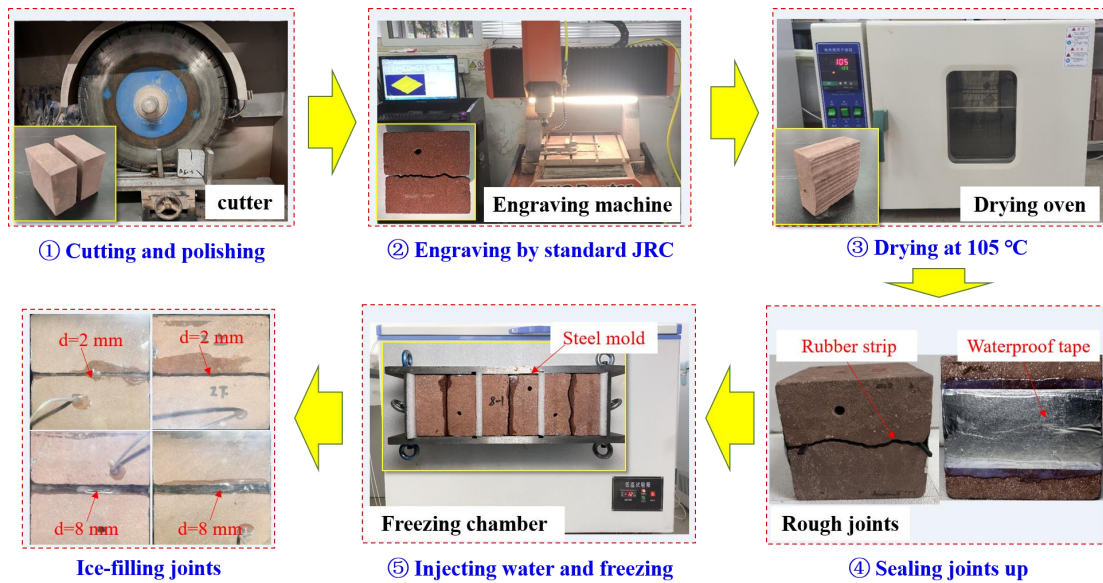
113

114    **Figure 1.**    Preparation of ice-filled joints. The preparation steps are as follows: ①  Cutting and polishing, ②

115    Engraving by standard, ③  Drying at 105 ℃, ④  Sealing joints up, ⑤  Injecting water and freezing.
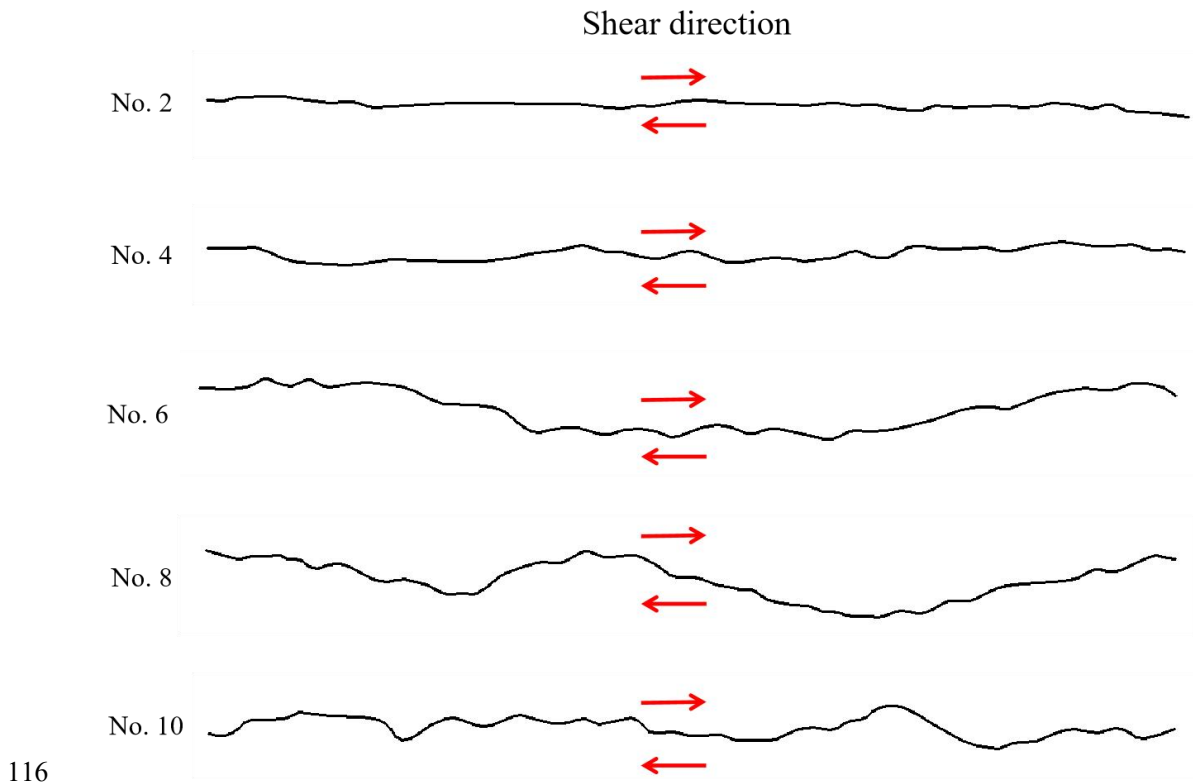
**Figure 2.** The shear directions for different joint profiles.

**2.3 Experimental procedures**

The main objective of this study is to investigate the effect of critical factors on the shear strength of ice-filled joint rock mass, including the freezing temperature, joint roughness, shear rates, joint opening and normal stress. The joint roughness is a basic index for rock joints, which is always considered when investigating other factors. Therefore, all the samples can be divided into 4 groups, namely the temperature group, shear rate group, joint opening group, and normal stress group. In the pre-test, the shear strength of the ice-filled joint does not change when the temperature is below -5 ℃, however, it greatly decreases when the temperature increases from -5 ℃ to 0 ℃. Therefore, the temperatures are set as -15 ℃, -5 ℃, -1 ℃ and -0.5 ℃, respectively. The shear rates are 0.2 mm/min, 0.4 mm/min and 0.8 mm/min in the shear rate group. In the joint opening group, the openings of ice-filled joints are 2

128 mm, 8 mm and 14 mm, respectively. The freezing depth on the earth may be small, however, it can

129 exceed 100 m in some alpine caves, where the in-situ stress is close to 2 MPa. Therefore, in the normal

130 stress group, the normal stresses are set as 0 MPa, 0.5 MPa, 1 MPa, 1.5 MPa and 2 MPa, respectively.

131 Three parallel experiments were performed on each group to eliminate the discreteness of ice-filled

132 joint samples and experiment error. There are approximately 225 ice-filled joint samples prepared in

133 this experiment. The distribution of these ice-filled joint samples were shown in Fig. 3.

134 All the water-containing joints were frozen in a freeze box at a specific temperature for about 12 h, and

135 they were used to conduct the direct shear experiment on a temperature-controlled shearing instrument

136 under the scheduled low temperature and normal stress (Fig. 4). A temperature sensor was implanted

137 into the sample to accurately monitor the internal temperature change of ice-filled joint samples. In

138 order to adjust the height of the ice-filled samples, a steel sheet was placed between the indenter and

139 joint blocks. When the scheduled freezing temperature was reached, the normal stress was applied with

140 a loading rate of 0.2 kN/s. Then the shear process was performed in the displacement mode with the

141 designed shear rate. After the shear experiment, the rupture modes of ice-filled joints were captured

142 and analyzed by using a camera.
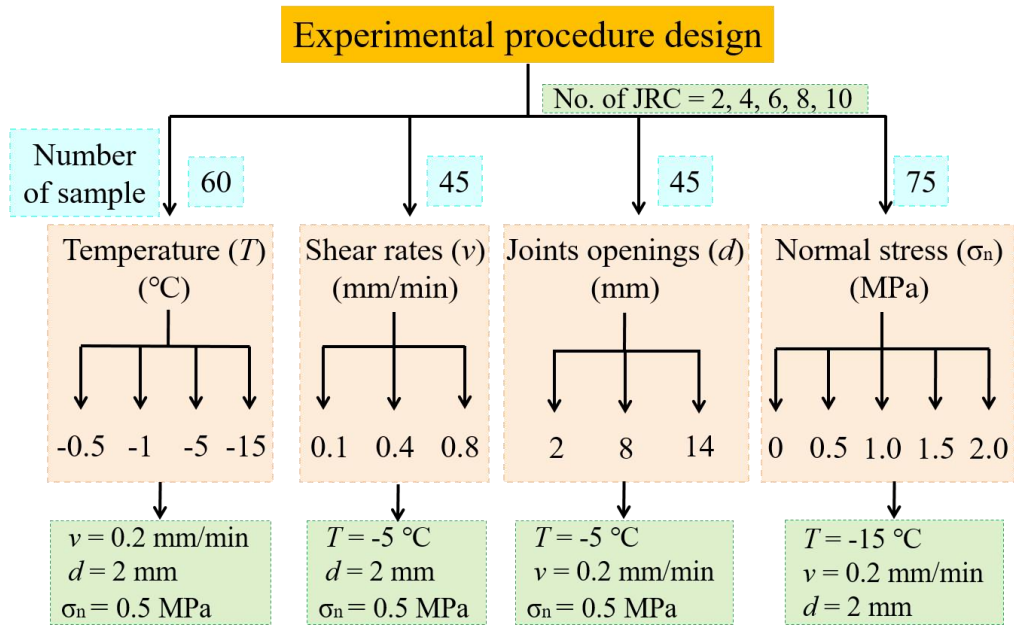
Figure 3. Distribution of rock samples containing ice-filled joints. $T$: Temperature. $v$: Shear rates. $d$: Joint openings. $\sigma_n$: Normal stress.
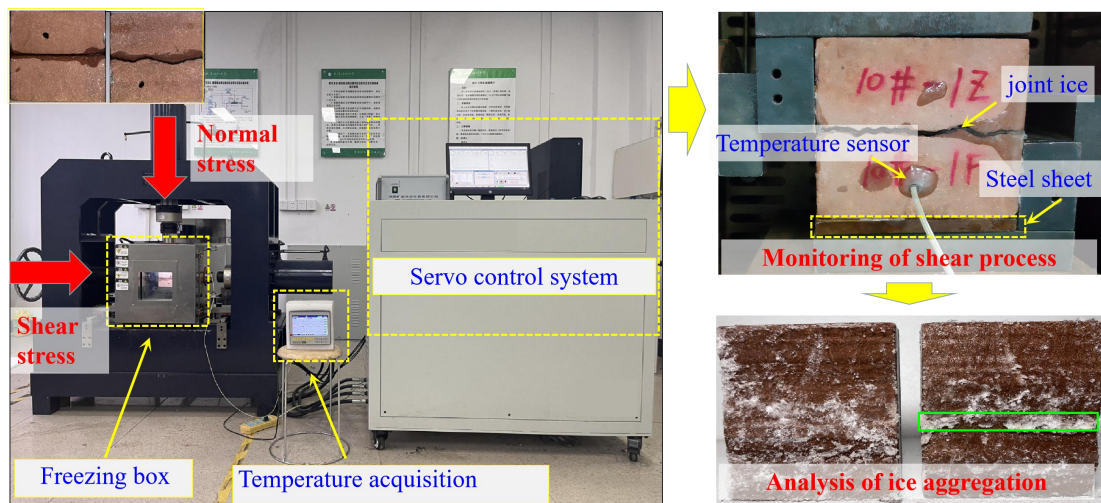
Figure 4. Shear experiment procedure and equipment

148 **3 Experimental results**

149 **3.1 Effect of freezing temperature and joint roughness**

150 In the temperature group, freezing temperatures were set as -15 °C, -5 °C, -1 °C and -0.5 °C, and the

151 joint roughness was named by the profile number in Table 2. The shear strength is dependent on the

152 freezing temperature and joint roughness as shown in Fig. 5. The shear strength decreases remarkably

153 with increasing freezing temperature. When the temperature increases from -15 °C to -0.5 °C, the mean

154 strength decreases by approximately 54%, 32%, 60%, 46% and 56% for profiles of No. 2, No. 4, No. 6,

155 No. 8 and No. 10, respectively. The shear strength of ice-filled joints does not always increase with

156 JRC, which has a considerable reduction at the joint profiles of No. 6 and No. 10. It illustrates that solid

157 ice is a kind of special infilled material, which is different from soft soils or cement-based materials

158 (Xu et al. 2012; Zhao et al. 2020). The change trend of shear strength against JRC may be explained by

159 the shear rupture mode, as shown in Fig. 6a. There are several aggregation regions of rupture ice close

160 to large climbing bulges on the surface of joints. The peak shear strength of ice-filled joints is related to

161 the aggregation area of rupture ice, because a large shear force is required to promote the solid ice to

162 shear slide along the slope of bulges. It should be noted that the rupture ice has a white appearance, low

163 transparency and obvious rupture characteristics by observing the enlarged pictures of the ice-filled

164 joints after shear failure. Only the rupture ice before the noticeable bulges displays aggregation

165 behavior. The area of the aggregation ice can be calculated after estimating the width of the

166 aggregation ice from the pictures (Fig. 6b), because the joints are two-dimensional surfaces. This is a

167 simple and approximate estimation method for the aggregation area of rupture ice.

168 The accumulated aggregation area percentage of the rupture ice can be calculated as

169 $$A_i = \frac{\sum_{k=1}^{n} L_k}{L_{\text{joint}}} \times 100\% \qquad (1)$$

170 where $L_k$ is the width of the aggregation ice for the bulge $k$. $L_{\text{joint}}$ =10 cm, which is the trace length of

171 the joint.

172 The aggregation area and location along the rough profile of joints after shear failure are plotted in Fig.

173 7. It can be observed that the aggregation ice appears before several high bulges and the aggregation

174 location is almost independent of the freezing temperature if aggregation ice occurs. The climbing

175 bulges in front of the aggregation ice are noticeable and influential. It implies that the influence of joint

176 roughness on the shear strengths of these ice-filled joints may be only controlled by several noticeable

177 bulges instead of the JRC index. Figure 8 shows that the shear strengths of No. 6 and No. 10 display

178 obvious reduction trends, which may be in accordance with the ice aggregation area. The ice

179 aggregation area decreases with increasing the freezing temperature, because the bonding strength

180 between ice and joint surface becomes to be weaker, and the shear rupture happens along the ice-rock

181 interface instead of solid ice when the freezing temperature is larger than -0.5 ℃.

182 In addition, when the freezing temperature is close to 0 ℃, the pre-melting of ice-rock interface

183 induced by the normal stress will cause a reduction of bonding strength. Therefore, the shear strength

184 between bonded ice-rock interfaces is much smaller than the shear strength of solid ice at a high

185 freezing temperature close to the melting point of bulk ice, such as -0.5 ℃. It should be noted that the

186 aggregation phenomenon of rupture ice disappears when $T$ = -0.5 ℃ because the high-temperature ice

187 is ductile failure along the ice-rock interface instead of the joint ice itself. However, the climbing effect

188 still makes a significant contribution to the increase of shear strength.

189
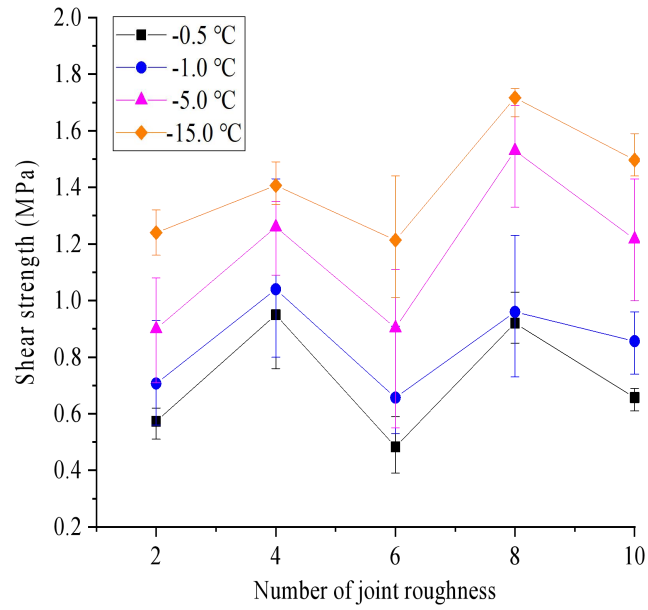
**Figure 5.** Shear strength against joint roughness at different freezing temperatures. Experimental condition: $v = 0.2$

191    mm/min, $d = 2$ mm, $\sigma_n = 0.5$ MPa.
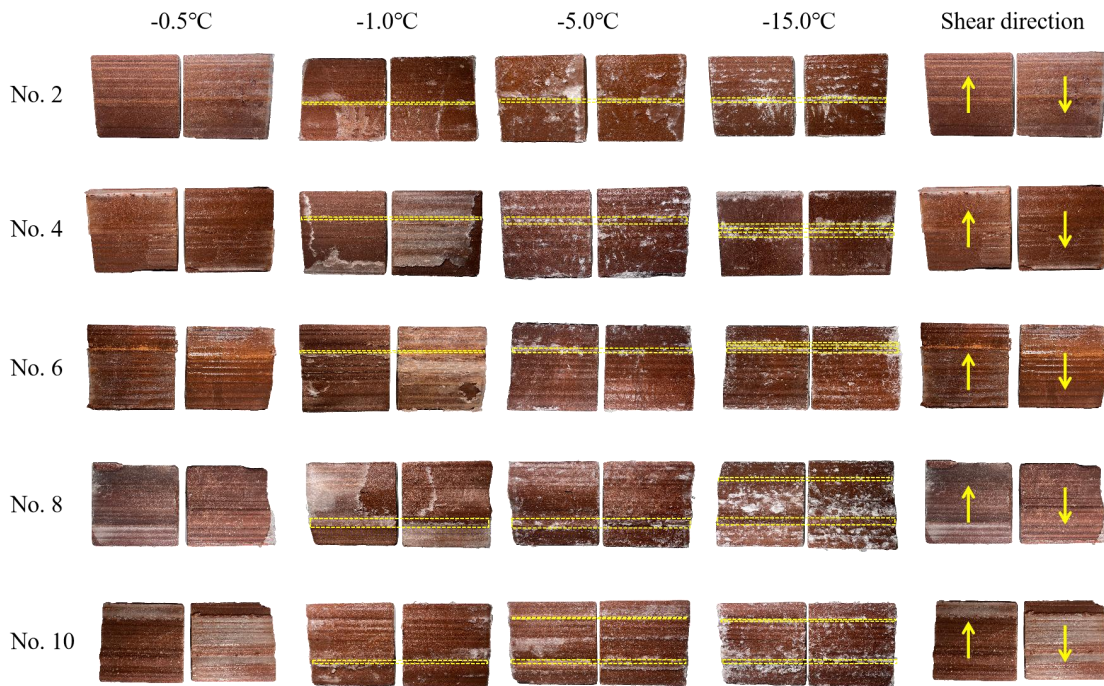
192

193                                    (a) Shear rupture modes
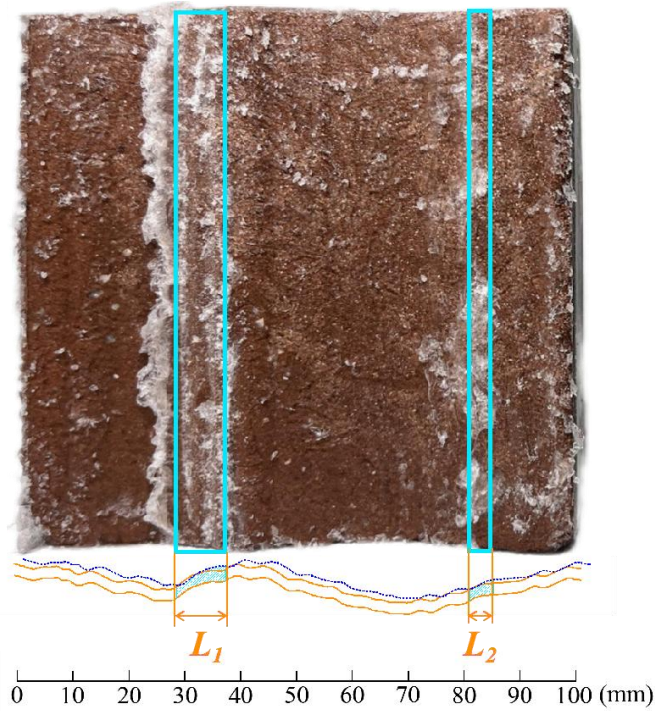
194

195       (b) Determination of the aggregation area of the rupture ice

196 **Figure 6.** Shear rupture modes and aggregation area of ice-filled joints at different freezing temperatures. The

197 yellow dotted lines show the main aggregation of rupture ice. Ice after rupture will aggregate in roughness bulges

198 perpendicular to the shear direction.

199

200

(b) No. 4

201

(c)  No. 6

202

(d) No. 8

(e) No. 10
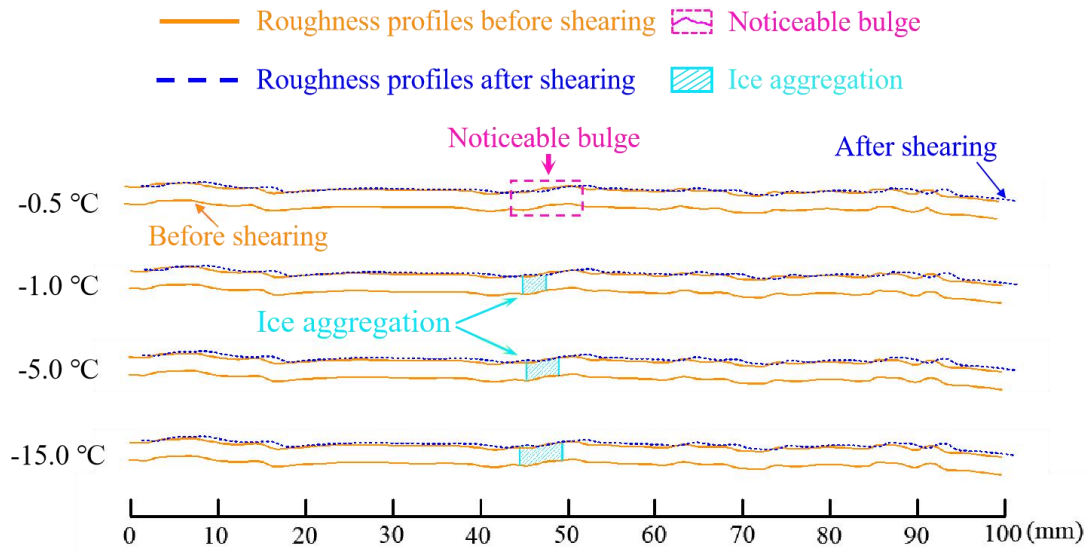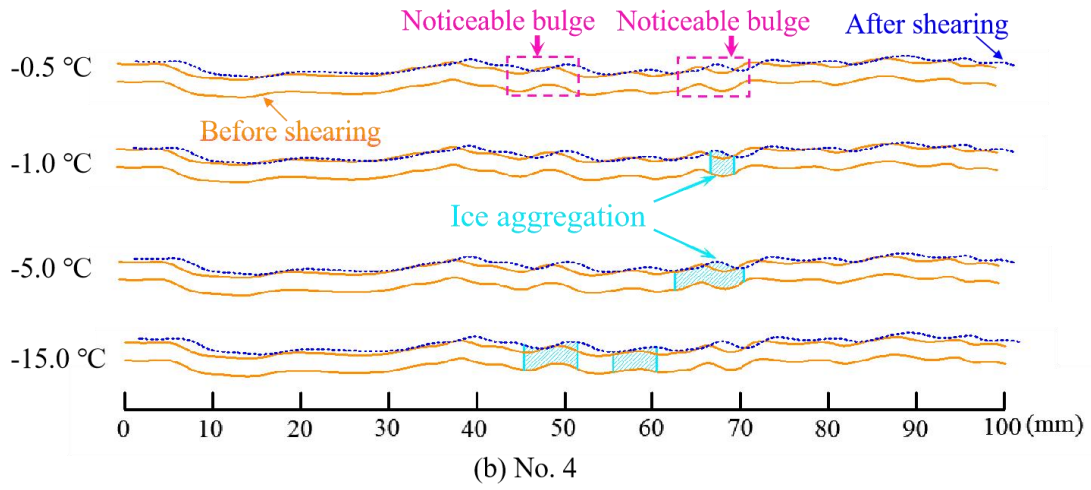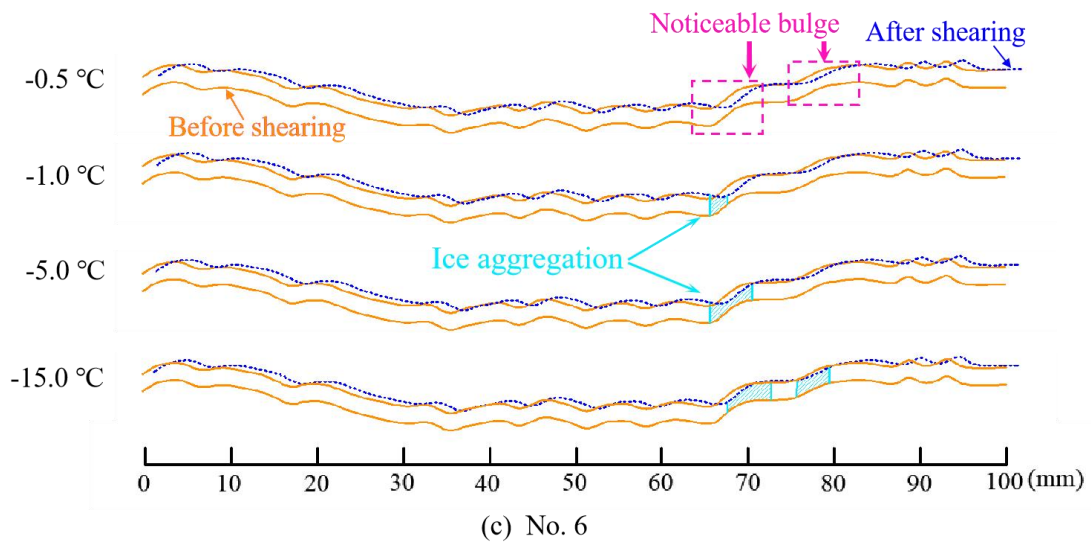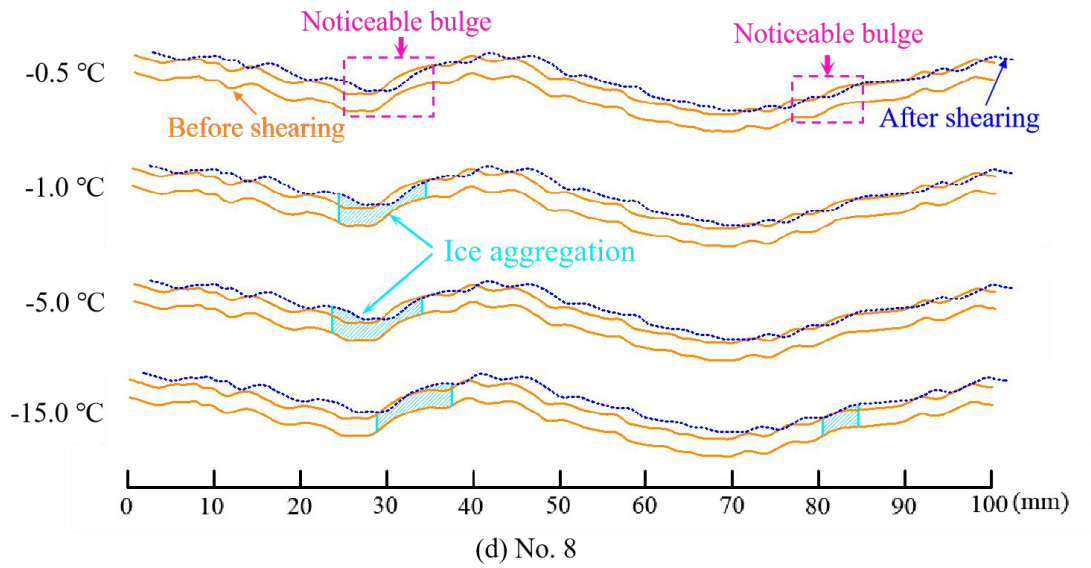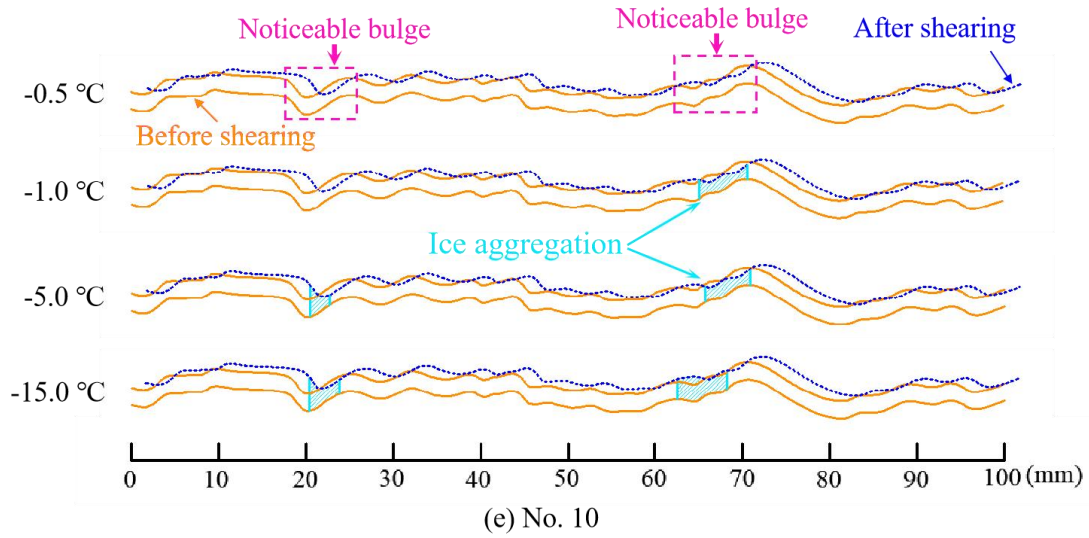
**Figure 7.** Shear aggregation areas of ice along the profile of roughness. Experimental condition: $v$ = 0.2 mm/min, $d$ = 2 mm, $\sigma_n$ = 0.5 MPa. Some blue profiles (dotted curves) are located under the orange profiles (solid curves) after shearing, which means the width of joints becomes smaller. Generally, the reduction of joint width occurs before some bulges and the rupture ice will aggregate before these bulges. The bulges causing the reduction of joint width and aggregation of ice are called noticeable bulges. The noticeable bulges have larger inclination angles and they are far away from the joint edges.
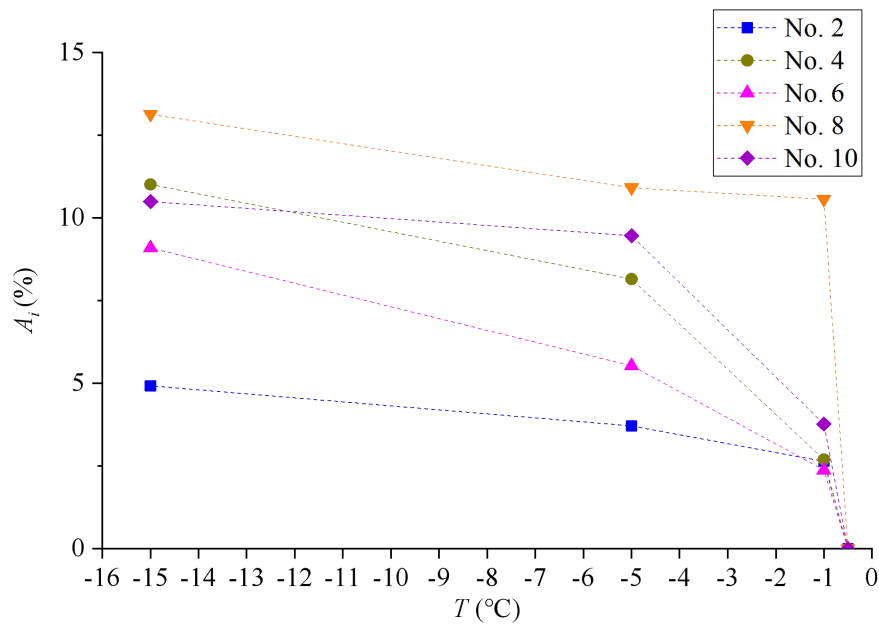
211 **Figure 8.** Aggregation area of rupture ice increases with the reduction of freezing temperature. Experimental

212 conditions: $v = 0.2$ mm/min, $d = 2$ mm, $\sigma_n = 0.5$ MPa. $A_i$: aggregation area percentage of rupture ice.

213 The peak shear displacement and normal displacement also are dependent on the freezing temperature

214 (Table 3 and Table 4). With the increase of freezing temperature, the peak shear displacement increases

215 because the joint ice will change from brittle to ductile (Bragov et al., 2015). The brittle-ductile

216 transition of pure ice also is related to the freezing temperature, and the rupture ice will be produced

217 under the brittle failure condition. Lou et al. (2022) claimed that plain ice has strong brittleness at the

218 temperature from -5 ℃ to -20 ℃. The increasing aggregation area of the rupture ice in Fig. 6 further

219 proves that the brittleness of ice increases with decreasing the freezing temperature. The maximum

220 shear displacement before failure is smaller at -15 ℃, which may be caused by the high brittleness.

221 When the temperature increases to -1 ℃, the solid ice becomes to be ductile, therefore a larger shear

222 displacement arises before failure. However, the shear dilatancy reduces with increasing the freezing

223 temperature. Solid ice is a kind of temperature-dependent material, the elastic modulus of which almost

224 linearly decreases with increasing freezing temperature (Sinha, 1989; Han et al. 2016). The inhibition

225 of normal stress on the shear dilatancy is greater at the high freezing temperature during the shear

226 process.

227 Several typical shear stress-displacement and normal-shear displacement curves for the profile of No. 4

228 are plotted in Fig. 9. The ice-filled joint shows significant residual shear strength beyond the peak point,

229 which slightly decreases with increasing shear displacement. This residual shear strength is caused by

230 the friction effect between the upper and lower ice-filled blocks. In addition, the normal shear dilatancy

231 displays increasing trend with shear displacement, which is caused by the climbing effect of ice-filled

232 joints. It should be noted that the shear strength has a second rising point at the residual strength stage,

233 because the shear rate is increased from 0.2 mm/min to 1 mm/min in order to accelerate the completion

234 of the shear process. Schulson and Fortt (2012) claimed that the friction between ice interfaces

235 increases when the shear rates increase from 0.06 mm/min to 0.6 mm/min. Therefore, the sudden rise

236 of residual shear strength can be attributed to the accelerated shear rate.

237 **Table 3.** The peak shear displacement at the peak points of shear strength (mm)

| Profile No. | Freezing temperature | | | |
|---|---|---|---|---|
| | -15 °C | -5 °C | -1 °C | -0.5 °C |
| No. 2 | 1.36 | 1.46 | 1.72 | 1.84 |
| No. 4 | 1.62 | 1.75 | 1.86 | 2.08 |
| No. 6 | 1.33 | 1.53 | 1.71 | 1.83 |
| No. 8 | 1.78 | 1.85 | 1.99 | 2.12 |
| No. 10 | 1.63 | 1.79 | 1.87 | 1.94 |

238

239 **Table 4.** The normal shear dilatancy at the point of peak shear strength (mm)

| Profile No. | Freezing temperature | | | |
|---|---|---|---|---|
| | -15 °C | -5 °C | -1 °C | -0.5 °C |
| No. 2 | 0.24 | 0.23 | 0.14 | 0.08 |
| No. 4 | 0.46 | 0.37 | 0.31 | 0.31 |
| No. 6 | 0.27 | 0.28 | 0.22 | 0.12 |
| No. 8 | 0.77 | 0.44 | 0.37 | 0.36 |

| No. 10 | 0.61 | 0.32 | 0.21 | 0.39 |
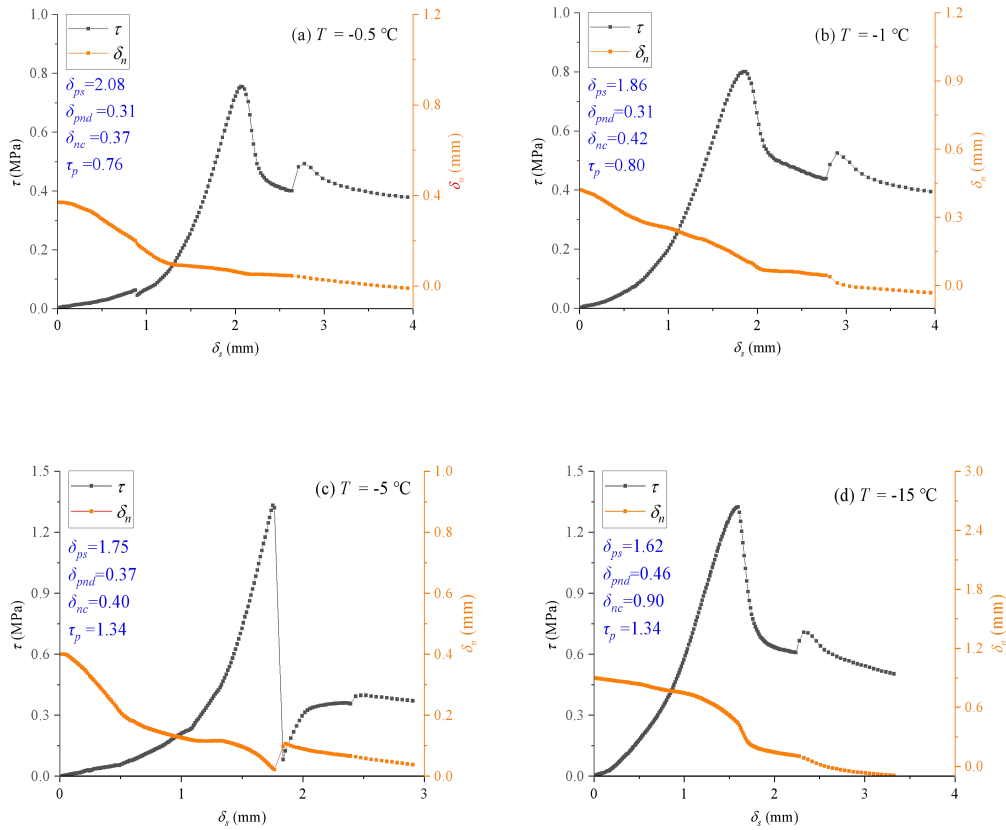
**Figure 9.** Shear strength and normal displacement versus the shear displacement for the profile of No. 4 in the temperature group. $\delta_{ps}$ and $\delta_{pnd}$ are the shear displacement and normal shear dilatancy at the point of peak shear strength, $\tau_p$ and $\delta_{nc}$ is the initial compression deformation.

Another finding is that the JRC is not suitable to interpret the influence of joint roughness on the shear strength of ice-filled joints, because the peak shear strength does not monotonically increase with increasing JRC index. The peak shear strength displays an increase-decrease-increase-decrease trend against JRC from No. 2 to No. 10 (Fig. 5). Figure 10 shows that the peak shear strength displays a linear increasing trend with increasing aggregation areas of fragmented ice after failure. The

251    aggregation area of fragmented ice can be treated as the effective climbing area which makes a

252    significant contribution to the improvement of shear strength, because the fragmented ice is produced

253    under compression-shear stress in the process of climbing the steep bulges. As a consequence, only

254    these steep bulges causing aggregation of rupture ice contribute to the improvement of shear strength.

255    The variation law of shear dilatancy against the roughness also is in accordance with the shear strength

256    of ice-filled joints, but it is different from the change law of JRC (Table 4). In Fig. 7, the gathering of

257    fragmented ice mainly arises in the front of the steepest bulge. It illustrates that the improvement of

258    shear strength of joint ice is caused by a part of the steepest bulge instead of the total roughness.

259    Therefore, JCR may be not suitable for the prediction of shear strength of ice-filled joints. For example,

260    although the JCR of No. 6 is much larger than No. 4, the effective steep bulge to cause ice aggregation

261    after failure is smaller than that of No. 4 (Fig. 8). This phenomenon confirms that the improvement of

262    shear strength is only caused by some noticeable steep bulges instead of the total bulges.

263
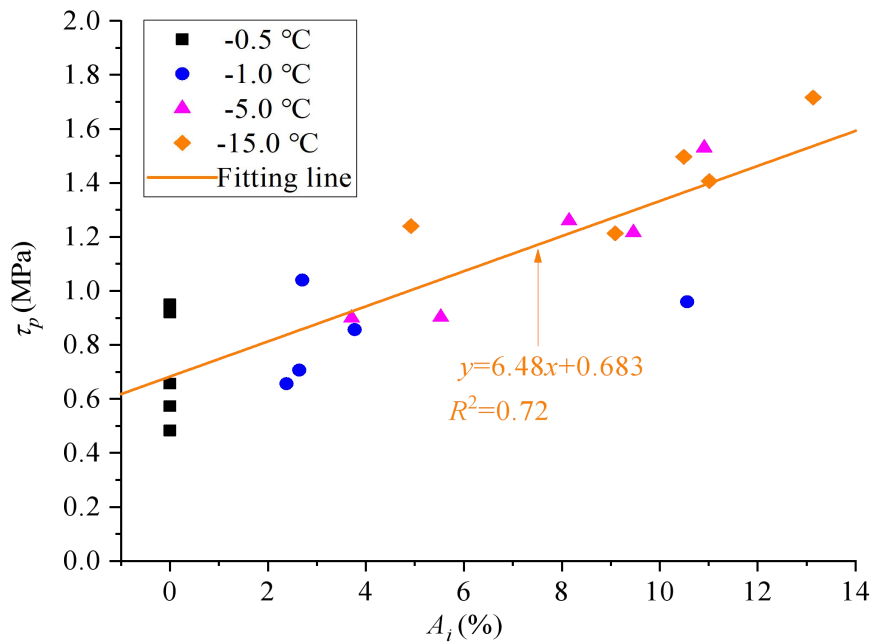
264    **Figure 10.** Peak shear strength linearly increases with increasing aggregation areas of rupture ice. Experimental

265    condition: $v$ = 0.2 mm/min, $d$ = 2 mm and $\sigma_n$ = 0.5 MPa.

266    **3.2 Effect of shear rates**

267    The shear rates have significant effects on the strength of solid ice as observed in the previous literature

268    (Petrovic, 2003). Low shear rates are used to conduct quasi-static shear experiments, including 0.2

269    mm/min, 0.4 mm/min and 0.8 mm/min. Figure 11 shows that the peak shear strength slightly decreases

270    with increasing shear rates. Solid ice is a kind of typical elasto-plastic material. When the shear rate is

271    slow, the ice crystal has enough time to shear slip and it will present ductile failure characteristics. At a

272    low shear rate, the free water on the slip interface will reorganize at the water-ice interface to form ice,

273    however, it is hard for the ice crystal to adjust to adapt the shear slip at high shear rates, which will

274    cause the shear rupture of ice crystals and hinder the growth of ice on the water-ice interface (Luo et al.,

275    2019). Mamot et al. (2018) claimed that a high strain rate of $10^{-3}$ $s^{-1}$ can induce brittle failure of ice and

276    rock-ice contacts. At a lower shear rate, the stress concentration inside infilled ice can be relaxed and it

277    changes to ductile creep deformation. Fukuzawa and Narita (1993) held that the brittle-ductile

278    transition of ice under the shear process occurs around the strain rate of $10^{-4}$ $s^{-1}$. Here, the shear

279    displacement rate is from 0.2 mm/min to 0.8 mm/min, corresponding to the strain rates from $1.67 \times 10^{-3}$

280    $s^{-1}$ to $6.67 \times 10^{-3}$ $s^{-1}$. Therefore, the shear rate in this study is very close to the threshold of brittle-ductile

281    transition given in the previous literature. Figure 12 shows that a high shear rate will induce brittle

282    failure of joint ice and more fragmented ice crystals are produced. As a result, the shear strength

283    reduces with increasing shear rates from 0.2 mm/min to 0.8mm/min. In this study, the exact shear rate

284    for the brittle and ductile transition of ice-filled joints is not accurately determined due to the limitation

285   of the shear rate range. More further shear experiments should be carried out on the ice and ice-filled

286   joints by adopting a larger range of the shear rate.
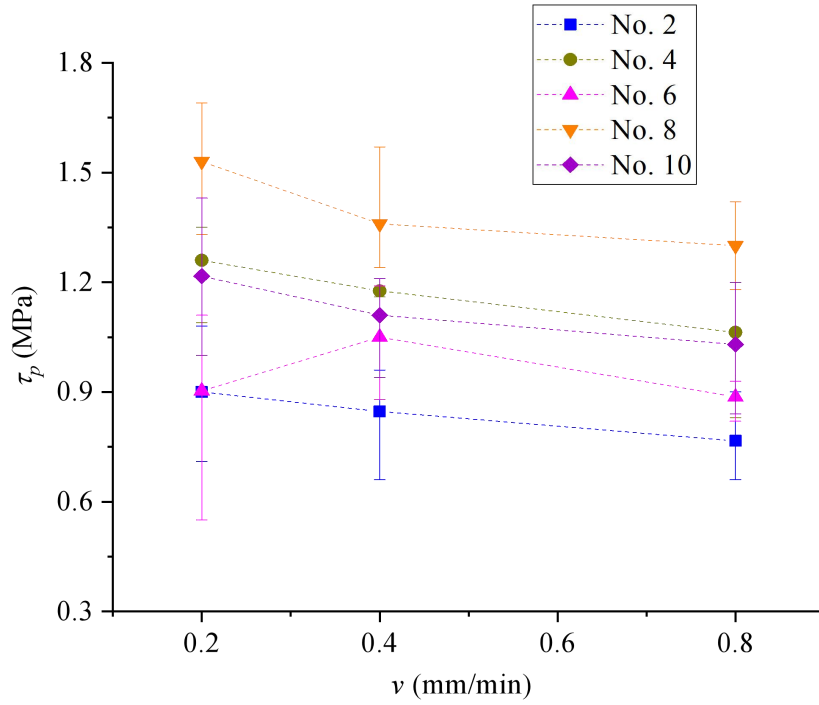
287

288   **Figure 11.** Effect of shear rate on the peak shear strength. Experimental condition: $T$ = -5 ℃, $d$ = 2 mm and $\sigma_n$ =

289   0.5 MPa.
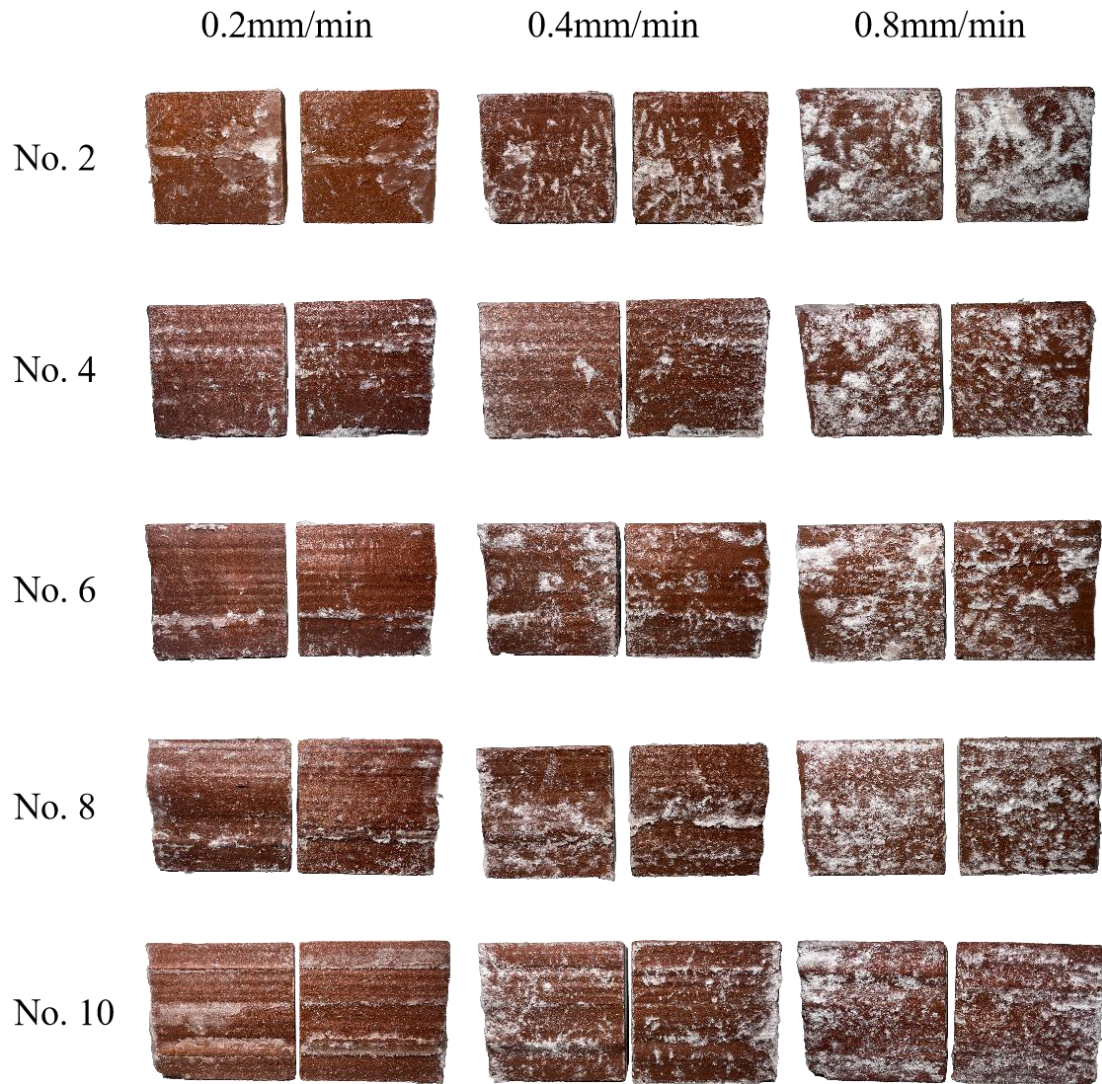
Figure 12. The shear rupture characteristics of joint ice under different shear rates. Experimental condition: $T =$ -5 °C, $d = 2$ mm and $\sigma_n = 0.5$ MPa. The ice crystal that cannot adapt to shear slip at high shear rates will form brittle failure. The joint ice of brittle failure shows more micro fractures which make it more reflective. This will cause a white appearance of the rupture ice on the joint surface. The ductile failure of ice displays a transparent appearance without white color, which is hard to observe. Therefore, a larger area of white appearance implies a much more serious brittle failure of joint ice.

## 3.4 Effect of joint openings

Joint opening is another critical factor influencing the shear strength of ice-filled joints, which is defined as the vertical distance between the upper and lower blocks. The standard JRC curves are suggested by Barton and Choubey (1977). We tested the maximum height difference of the standard JRC curves is approximately 2.14 mm, 2.40 mm, 6.24 mm, 6.85 mm and 4.48 mm for the profiles of No. 2, No. 4, No. 6, No. 8 and No. 10, respectively. The joint openings are chosen as 2 mm, 8 mm and 14 mm, because 2 mm is smaller than all the maximum height differences while 14 mm is much larger than them. The rupture characteristics of joint ice against the joint opening are plotted in Fig. 13. When the joint opening is 2 mm, the aggregation phenomenon of rupture ice is evident. However, the aggregation phenomenon disappears for the profiles of No. 2, No. 4 and No. 6 when the joint opening is 8 mm. When the joint opening increases to 14 mm, there is not any aggregation of rupture ice arising for all the joints. Figure 14 shows that when the joint opening increases from 2 mm to 14 mm, the shear strength of ice-filled joints decreases. The shear strength of pure solid ice also is measured in the laboratory, which is approximately 0.83 MPa on the condition that $T = $ -5 °C, $v = 0.2$ mm/min and $\sigma_n = 0.5$ MPa. When the joint opening is 14 mm, the shear strengths of ice-filled joint are approximately 0.83 MPa and they are independent of the joint roughness. When the joint opening is 8 mm, the shear strengths of ice-filled joint are very close to the shear strength of pure solid ice (0.83 MPa) for the joint of No. 2, No. 4 and No. 6. The reason is that 8 mm has exceeded the critical filling thickness of these joints (No. 2, No. 4 and No. 6), therefore the shear strength of these ice-filled joints is only controlled by the solid ice instead of joint roughness. In addition, there is not any significant ice aggregation on the joint surfaces of No. 2, No. 4 and No. 6 when the joint opening is 8 mm, and the shear failure

319     happens inside the joint ice. However, for the ice-filled joints of No. 8 and No. 10, the shear strengths

320     are larger than 0.83 MPa, which illustrates that the critical filling thickness for the profiles of No. 8 and

321     No. 10 should be larger than 8 mm but smaller than 14 mm. There is aggregation ice arising before

322     large bulges, and these large bulges would prevent the direct shear failure of joint ice and improve the

323     shear strength.

324     The influence of joint opening and roughness on the shear strength can be explained by using the shear

325     failure path of ice-filled joints as shown in Fig. 15. When $d$=2 mm, the shear climbing will occur before

326     some large bulges for all the joint profiles. This climbing action induces the aggregation of rupture ice

327     and change of shear path. As a consequence, the shear strength will improve. When $d$=8 mm, the shear

328     failure path will not be disturbed for the profiles of No. 2, No. 4 and No. 6, however, the shear failure

329     path changes due to the climbing action for the profiles of No. 8 and No. 10, in which a significant

330     aggregation of rupture ice is produced. Therefore, the shear strengths of ice-filled joints for the profiles

331     of No. 2, No. 4 and No. 6 are approximately equal to the solid ice, while the shear strengths for the

332     profiles of No. 8 and No. 10 are much larger than 0.83 MPa. When $d$ = 14 mm, the shear failure

333     happens inside the joint ice for all joint profiles, therefore, the shear failure path and shear strength will

334     not be influenced by the joint roughness and no aggregation of rupture ice occurs. The shear dilatancy

335     deformation of the ice-filled joints in Fig. 16 has further proved the climbing actions, including all the

336     profiles with joint opening of 2 mm, and the profiles of No. 8 and No. 10 with joint opening of 8 mm.

337     The climbing effect of the No. 2 ice-filled joint with opening of 2 mm is not remarkable, therefore the

338     shear dilatancy is very small and the shear strength also is close to pure solid ice (0.83 MPa).

339     Regardless of the critical filling thickness, the present study shows that the shear strength of ice-filled

340 joints decreases with increasing joint openings from 2 mm to 14 mm, and it is related to the joint

341 roughness below the critical infilled thickness. When the filling ice exceeds the critical thickness, the

342 shear strength of ice-filled joints is equal to the shear strength of solid ice under the same condition. It

343 should be noted that the critical filling thickness for each roughness will be determined in future

344 studies.
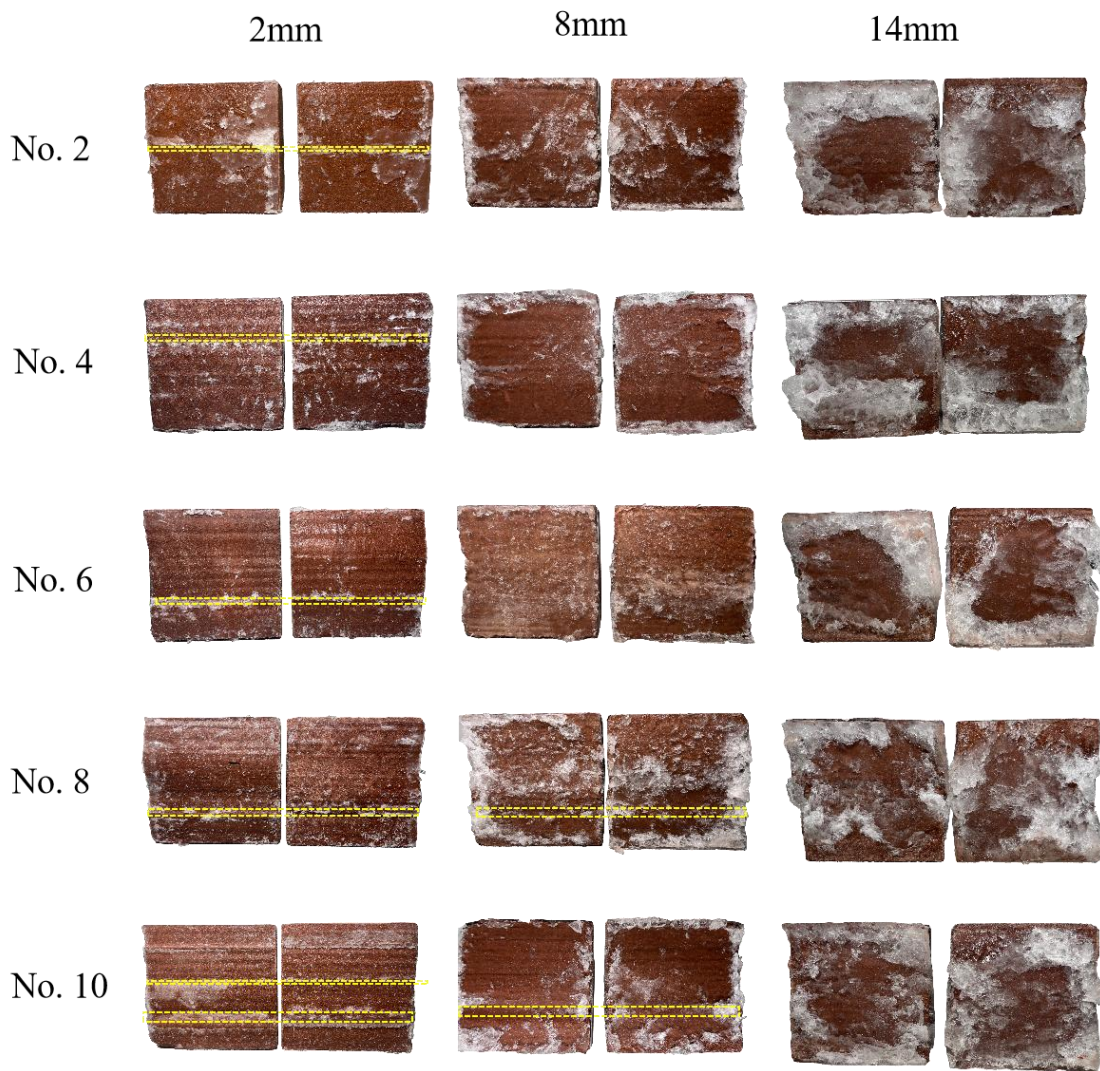
346 **Figure 13.** The shear rupture characteristics of ice-filled joints with different openings. Experimental condition: $T$

347 = -5 °C, $d$ = 2 mm and $\sigma_n$ = 0.5 MPa. The yellow lines show the main aggregation of rupture ice. Ice after rupture

348 will aggregate in roughness bulges perpendicular to the shear direction. The aggregation phenomenon disappears

349      as the joint openings increase. The aggregation phenomenon of profiles No. 2, No. 4 and No. 6 disappear in 8 mm

350      joint openings. All profiles' aggregation phenomena disappear in 14 mm joint openings.
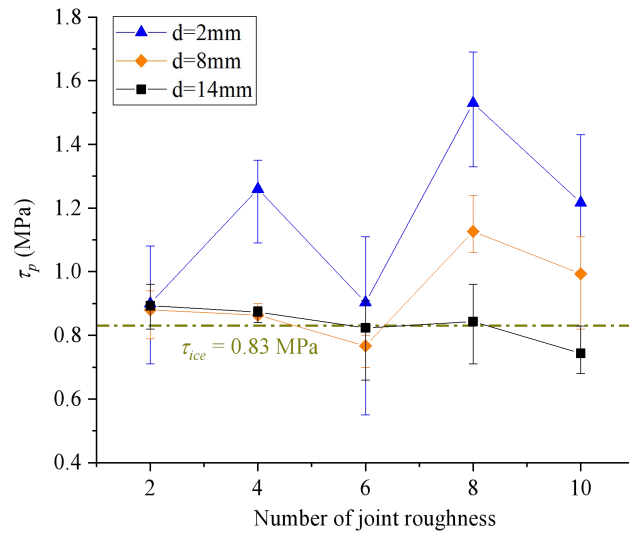
351

352      **Figure 14.** Effect of joint opening on the peak shear strength. Experimental condition: $T$ = -5 °C, $v$ = 0.2 mm/min

353      and $\sigma_n$ = 0.5 MPa.

354
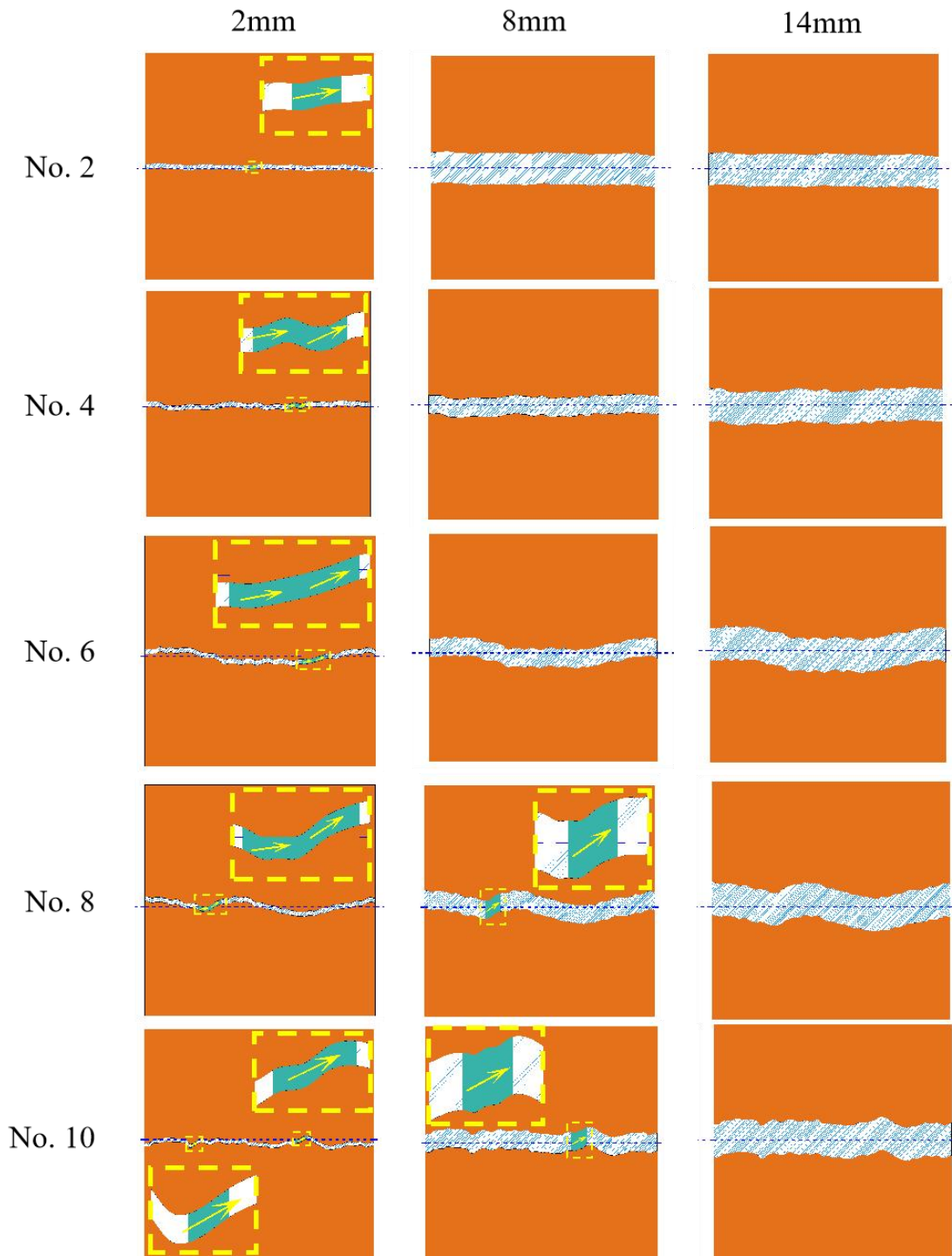
**Figure 15.** Influence of joint roughness on the shearing slip path. Experimental condition: $T$ = -5 ℃, $v$ = 0.2

356    mm/min and $\sigma_n$ = 0.5 MPa.

357

358
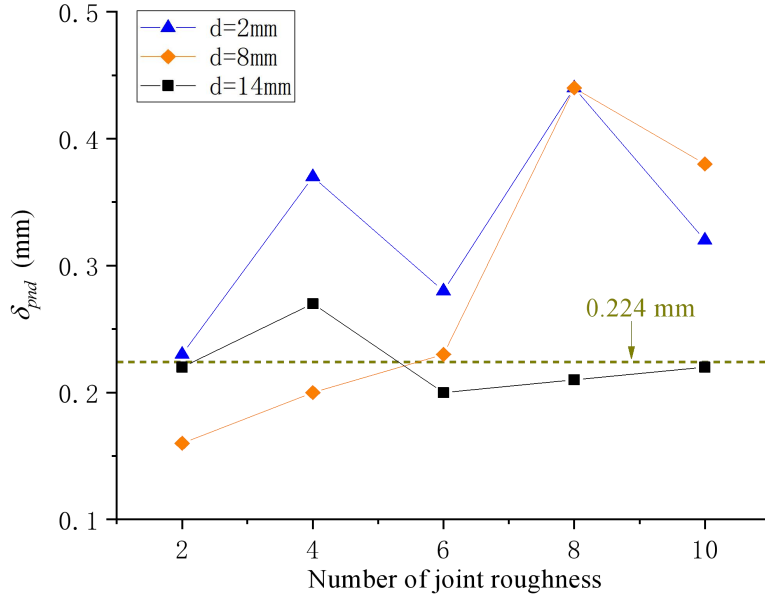
**Figure 16.** Effect of joint opening on the shearing dilatancy. Experimental condition: $T$ = -5 °C, $v$ = 0.2 mm/min

and $\sigma_n$ = 0.5 MPa.

**3.5 Effect of normal stress**

The normal stress group was used to investigate the effect of normal stress on the shear strength of

ice-filled joints, including 0 MPa, 0.5 MPa, 1.0 MPa, 1.5 MPa and 2.0 MPa. The shear strength of

ice-filled joints displays a significant increasing trend with increasing normal stress (Fig. 17). The

Mohr-coulomb criterion may be used to express the relationship between the shear strength and normal

stress as below:

$$\tau_p = c_j + \sigma_n \tan \phi_j \tag{2}$$

where $\tau_p$ = shear stress on plane, $\sigma_n$ = normal stress on plane, $c_j$ = cohesion of ice-filled joints,

$\phi_j$ = internal friction angle of ice-filled joints.

Figure 17 shows Mohr-coulomb criterion can be well used to calculate the shear strength of ice-filled

joints against the normal stress. The shear rupture modes of the joint ice are given in Fig. 18. A

372  remarkable ice aggregation phenomenon can be found on the surface of joints and the aggregation

373  occurs at a stable location of the joint profile regardless of the normal stress. The aggregation area of

374  rupture ice increases with increasing normal stress, because climbing bulges is harder and the solid ice

375  is easier to be crush at the front of large bulges under the higher normal stress (Fig. 19). In Section 3.1,

376  it has illustrated that the aggregation area of rupture ice is an important index to reflect the shear

377  strength of ice-filled joints at different freezing temperatures. Actually, the shear strength also linearly

378  increases with increasing the aggregation area of rupture ice under different normal stress as shown in

379  Fig. 20. It further illustrates that only some large bulges causing the aggregation of rupture ice can

380  contribute to the improvement of shear strength instead of the total roughness index, such as JRC.

381

382

383

384

385
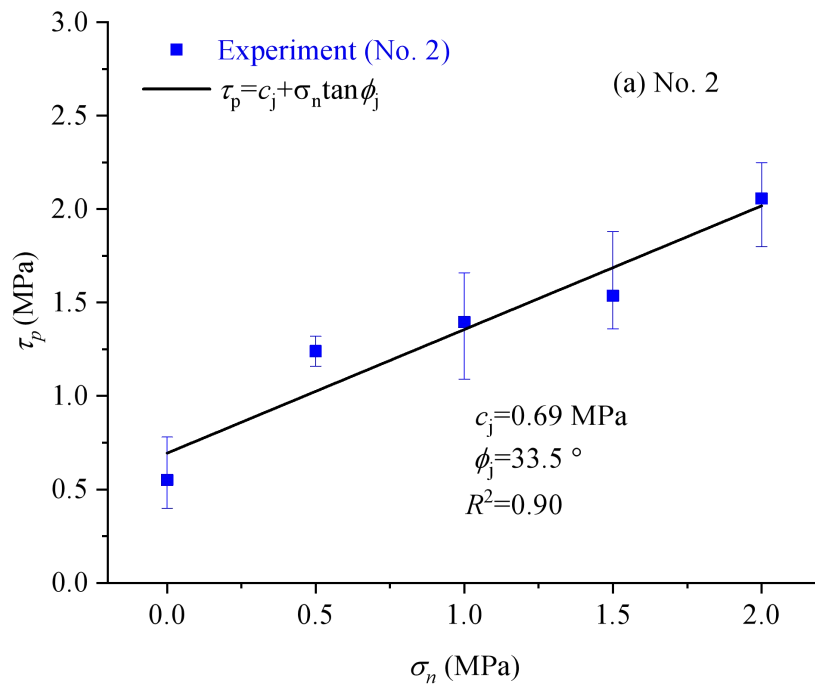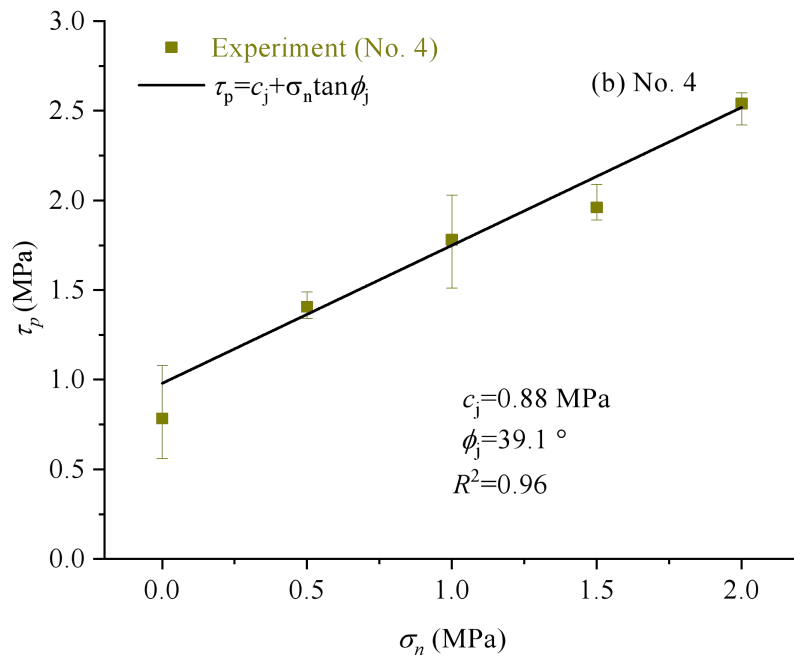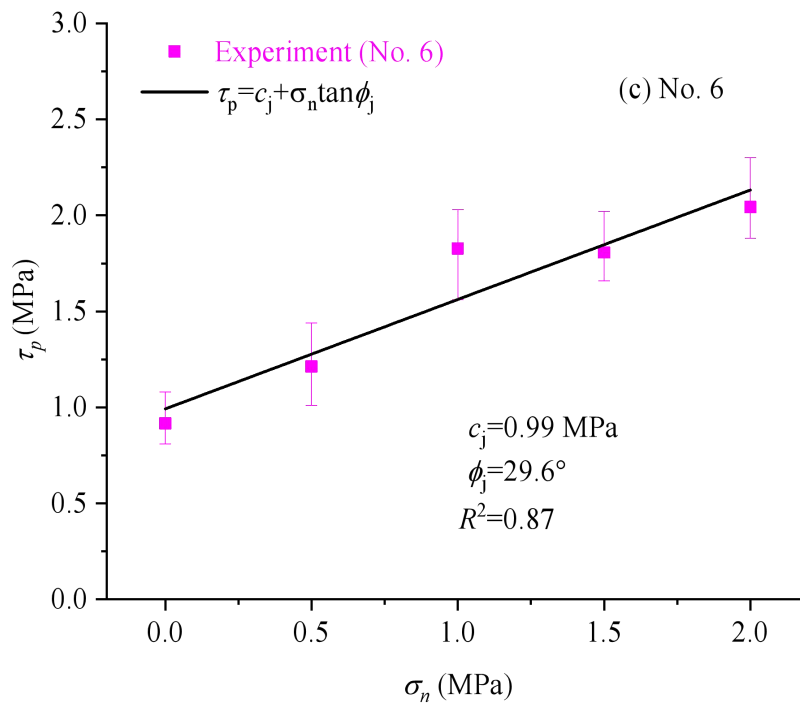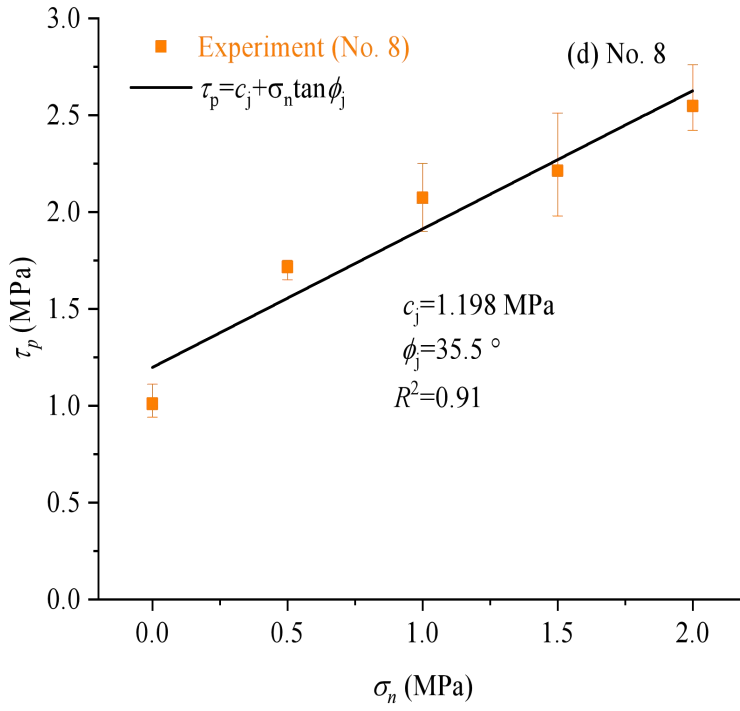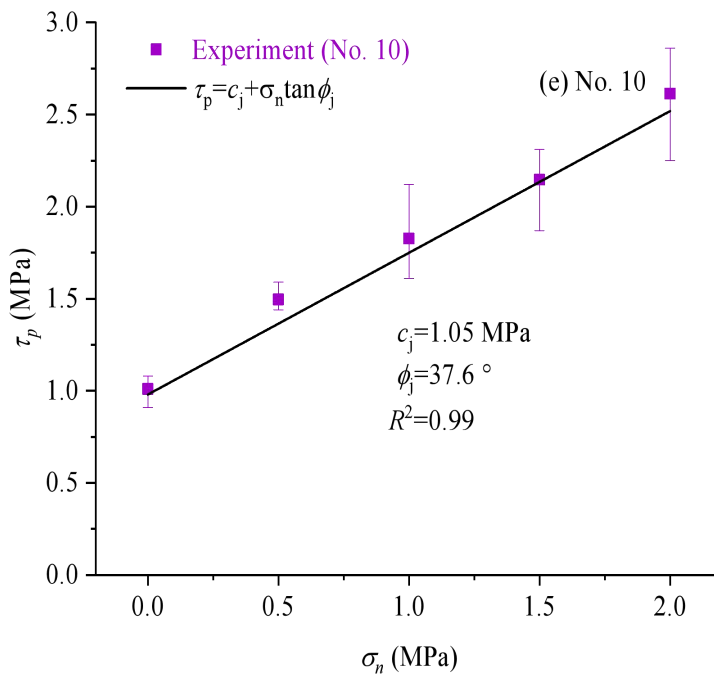
**Figure 17.** Effect of normal stress on the peak shear strength of ice-filled joints. Experimental condition: *T* =

387    -15 °C, *v* = 0.2 mm/min and *d* = 2mm.

388
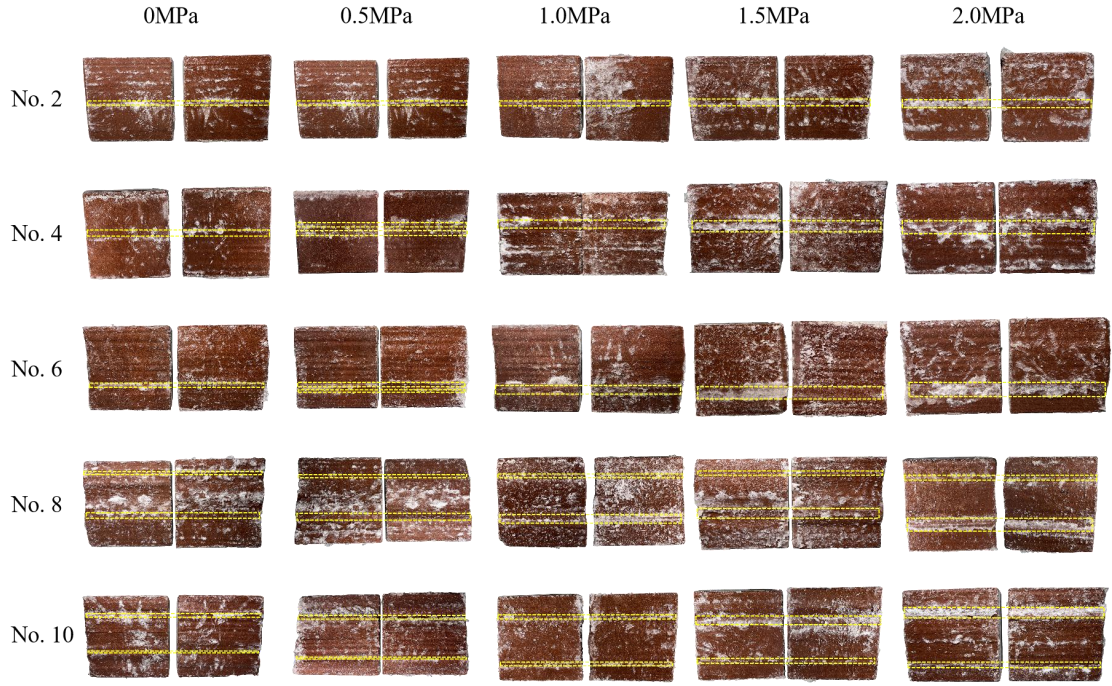
**Figure 18.** Aggregation of rupture ice under different normal stresses. Experimental condition: $T$ = -15 °C, $d$ = 2

390    mm and $v$ = 0.2 mm/min. The yellow lines show the main aggregation of rupture ice.

391
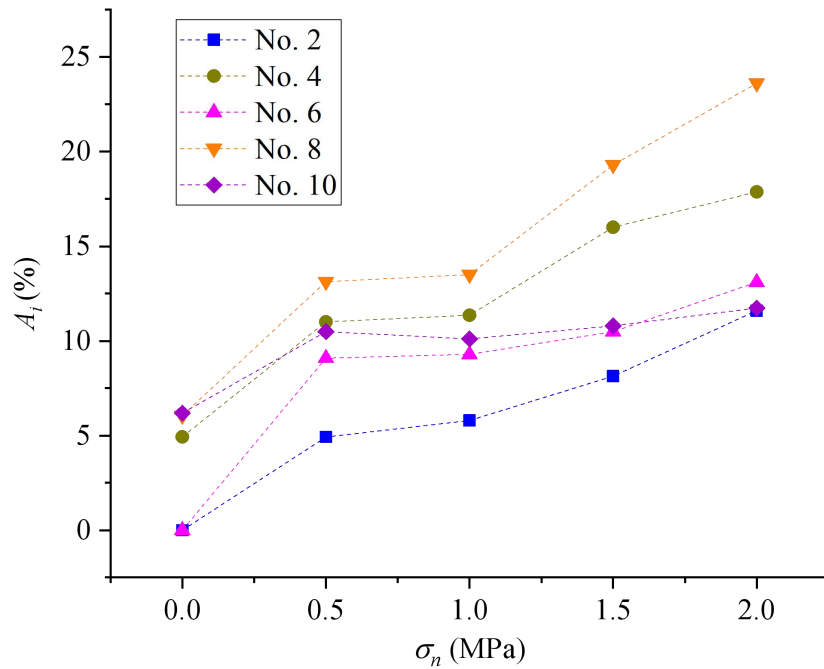
**Figure 19.** Aggregation area of rupture ice increases with increasing normal stress. Experimental condition: $T$ =

393    -15 °C, $d$ = 2 mm and $v$ = 0.2 mm/min.

394
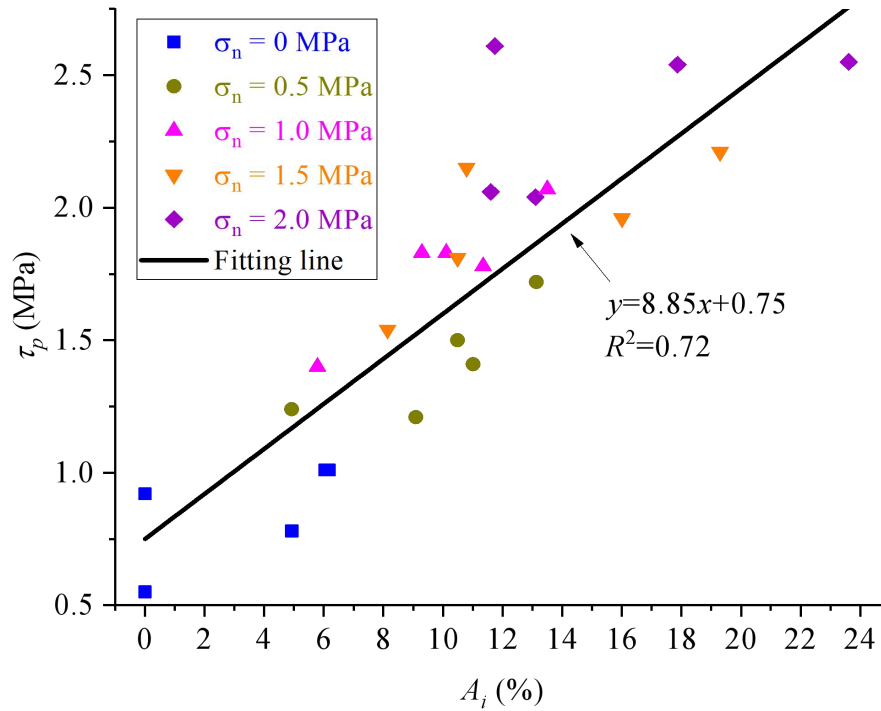
**Figure 20.** Peak shear strength linearly increases with increasing aggregation areas of rupture ice. Experimental

condition: $T$ = -15 °C, $d$ = 2 mm and $v$ = 0.2 mm/min.

## 4. Discussion

### 4.1 The warming degradation mechanism of ice-filled joints

In this paper, the influence of freezing temperature, shear rate, joint opening and normal stress on the

shear strength of ice-filled joints in rock masses was comprehensively investigated by experiments. The

shear strength remarkably reduces with increasing freezing temperature, because the shear strengths of

solid ice and ice-rock interface decrease with increasing temperature. In order to deeply understand the

warming degradation mechanism of ice-filled joints, the shear strength of pure ice and ice-rock

bonding interface under different freezing temperatures also were tested in this study (Fig. 21).

405     The test results show that the shear strength of smooth ice-rock bonding interface is larger than that of

406     pure solid ice at the freezing temperature from -15 to -0.5 °C (Fig. 21a). It implies that the shear failure

407     should be inside the solid ice instead of ice-rock interface. When the freezing temperature increase

408     from -1 °C to -0.5 °C, the shear strengths of the ice-rock interface and the solid ice reduce very quickly.

409     Jia et al. (2015) also claimed the same change law of solid ice against the temperature.

410     However, the experimental results show that the shearing failure of many rough ice-filled joints at

411     -0.5 °C is the debonding of ice-rock interfaces (Figs. 6, 12, 13, 18). More shear experiments were

412     carried out on rough ice-rock interfaces with profiles of No. 4 and No. 8 on the same experimental

413     condition ($\sigma_n$ = 0.5 MPa, $v$ = 0.2 mm/min). It shows that the shear strength of rock-ice-rock "sandwich"

414     is a little larger than that of ice-rock interface, although the change laws of them against temperature

415     are very similar. Another novel finding is that the shear strength of ice-rock interface is larger than the

416     shear strength of solid ice itself below -1 °C (Fig. 21b). Therefore, the shear failure below -1 °C

417     displays the cracking of joint ice instead of ice-rock interface, and some aggregation areas of rupture

418     ice occur before large bulges (Figs. 6, 12, 13, 18). However, the shear strength of solid ice is larger

419     than that of ice-rock interface above -1 °C. This is the main reason for the shear failure of rough

420     ice-filled joints along ice-rock interfaces at -0.5 °C. The freezing temperature of -1 °C is the transition

421     point of shear failure modes. Figure 22 presents that the shear failure is along the ice-rock interface

422     when the freezing temperature is approximate -0.5 °C, however, the area of ice attached to the joints

423     has a great increment with the decrement of freezing temperature from -0.5 °C to -15 °C. It further

424     illustrates that the shear strength of rough ice-rock interface is larger than that of the solid ice below

425     -5°C. Mamot et al. (2018) also found that the shear failure modes of the smooth ice-filled joints

426 changed from shearing cracking of joint ice to the debonding of ice-rock interface when the freezing

427 temperatures increased from -10 ℃ to -0.5 ℃. The smooth joints have a little ability to resist the shear

428 slide of ice-filled joints. Mamot et al. (2018) claimed that three shear failure modes may arise between

429 -5 ℃ to -1 ℃, including the debonding of ice-rock interface, shear cracking of joint ice and their mixed

430 mode. However, only the shear cracking of joint ice occurs at -5 ℃ to -1 ℃ in this study. Therefore,

431 the joint roughness has an effect on the shear strength of ice-filled joints and the shear failure modes.

432
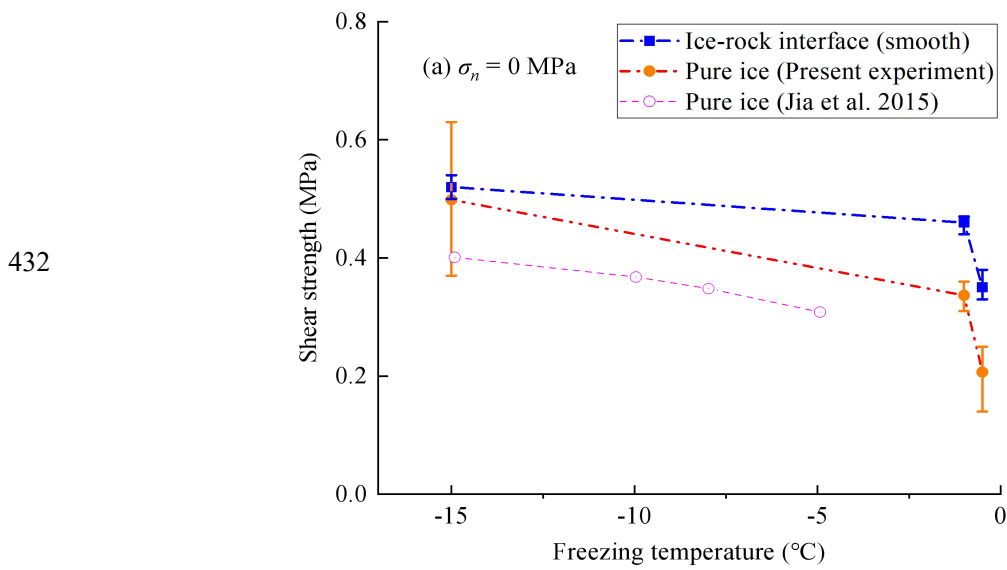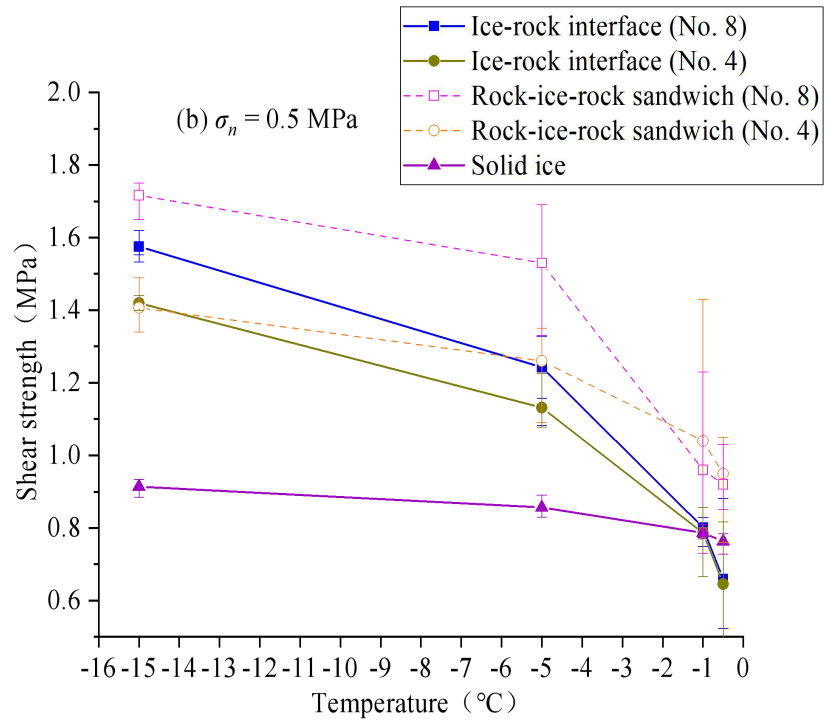
**Figure 21.** Influence of freezing temperature on the direct shear strength of ice and ice-filled joints. Experimental
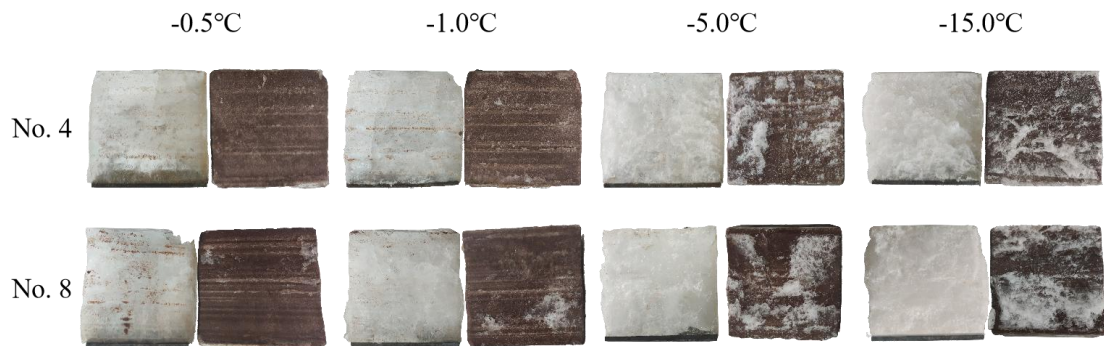
condition: $v$ = 0.2 mm/min.

**Figure 22.** Shear failure characteristics of ice-rock interfaces under different temperatures. Experimental condition:

$v$ = 0.2 mm/min, $\sigma_n$ = 0.5 MPa.

**4.2 The coupled effect of joint roughness, opening and normal stress**

The shear strength of smooth ice-filled joints were investigated by Mamot et al. (2018). They found

that the shear strength of smooth ice-filled joints also linearly increases with decreasing temperatures.

Actually, the roughness is another important factor influencing the shear strength of ice-filled joints,

which can improve the ability to resist the shear slide of joints (Fig. 23). The shear strength of the No. 2

ice-filled joint is much smaller than that of No. 8 and No. 10 joints. For the profile of No. 2, the shear

strength of ice-filled joint is approximately equal to that of the solid ice when the normal stress is less

than 1.5 MPa, because the joint opening of 2 mm also is very close to the maximum height difference.

Therefore, the joint opening will determine the effect of joint roughness. However, the shear strength of

solid ice is much smaller compared with the shear strength of ice-filled joints when the normal stress is

2 MPa. It is observed that this normal stress has caused some vertical micro-cracks inside the solid ice.

For the ice-filled joints, the compression damage maybe not remarkable, because both the adhesion of

ice-rock interface and bulges will prevent the lateral expansion of solid ice under high normal stress. A

larger roughness may provide a much stronger confining effect on the lateral expansion. Although the

shear strength increases with increasing JRC number in general, the quantitative relationship between

them are hard to determine. Figure 5 shows that the change of shear strength against the JRC number is

fluctuating. A novel finding of this study is that the aggregation area of rupture ice before large bulges

can be well used to predict the shear strength of ice-filled joints. However, it should be noted that a

new index of roughness should be proposed in future research in order to build the shear strength

model considering joint roughness.

460 In addition, if the joint opening exceeds the critical value, the influence of joint roughness on the shear

461 strength of ice-filled joints will disappear. For example, when the thickness of joint ice exceeds 14 mm,

462 the shear strength of all the ice-filled joints is equal to the shear strength of infilled ice. Section 3.4 has

463 illustrated that the value of critical joint opening is depended on the maximum height different of the

464 joint, which need to study further.
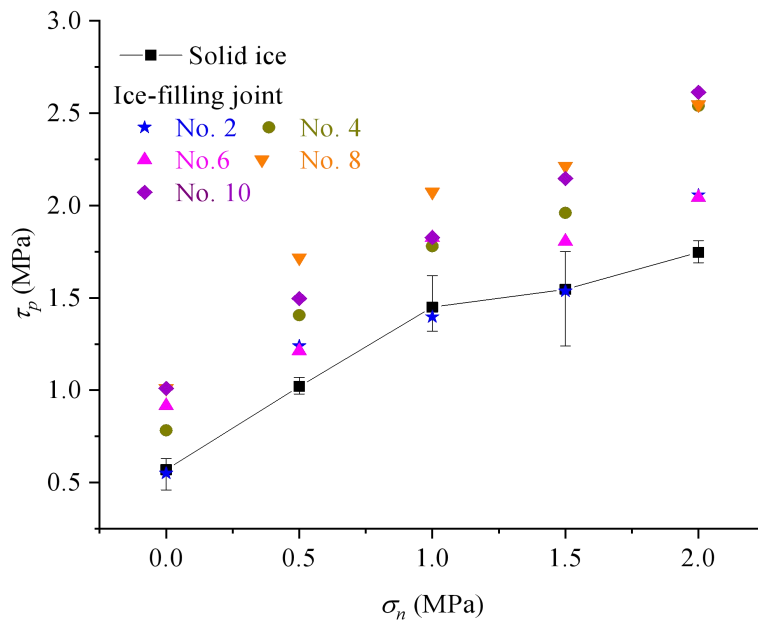
465

466 **Figure 23.** Shear failure characteristics of ice-rock interfaces under different normal stress. Experimental condition:

467 $v = 0.2$ mm/min, $d = 2$ mm, $T = -15$ ℃.

468

469 **4.3 Potential application for prediction of rock avalanches in a warming climate**

470 In recent years, there are many large rock avalanches occurred in the Alps. The rock avalanches that

471 occurred on the Brenva galcier, the Punta Thurwieser and the Drus are some of the recent examples,

472 which have strong impacts on the high mountain infrastructure stability and landscape evolution

473 (Mamot et al., 2018). The rock avalanches are related to the degradation of bedrock permafrost and

474     ice-filled joints. Our study shows that the peak shear strength of ice-filled joints increases with the

475     increase of roughness and normal pressure. This implies that the rockfall will be more stable with

476     higher roughness and normal pressure. In addition, when the joint openings increase, the peak shear

477     strength will decrease, and large joint openings will reduce the effect of joint roughness. The peak

478     shear strength of ice-filled joints decreases with the increase of freezing temperature. Moreover, when

479     the freezing temperature is close to 0 ℃, the pre-melting of ice-rock interface induced by the normal

480     stress will cause a reduction of bonding strength. This result can explain the phenomenon that the

481     boundary of ice-filled joint between frozen and unfrozen become unstable, especially in summer. The

482     peak shear strength of ice-filled joints decreases with the increase of shear rate. It is hard for the ice

483     crystal to adjust to adapt the shear slip at high shear rates so the rockfall may happen.

484     As the global temperature rises, collapse disasters of ice-filled rock mass caused by warming and

485     thawing often occur in permafrost regions. A constitutive model can be further constructed according

486     to the experiment results. Then combining with a numerical software, this constitutive model can be

487     used to predict the disaster of rock avalanches in the cold region in the future research. Although

488     Mamot et al. (2018) has established a constitutive model for joints, the constitutive model only

489     considers temperature and normal stress, however, the influence of the joint roughness, opening and

490     shear rate is ignored. Through our study, it is evidenced that the joint roughness, shear rate, joint

491     opening and temperature are physical quantities that must be considered in the constitutive model. A

492     constitutive model including these physical quantities will be proposed in our future research.

493     **5 Conclusions**

494     The following conclusions can be obtained in this study:

(1) The shear strength of ice-filled joints decreases with increasing temperature. The shear failure mode change from shear rupture of joint ice to the debonding of ice-rock interface when the temperature increases to -0.5 °C, because the bonding strength of ice-rock interface is less than that of solid ice at -0.5 °C ($v = 0.2$mm/min, $\sigma_n = 0.5$ MPa).

(2) The joint roughness can improve the shear strength of ice-filled joints, but it is related to the joint opening and normal stress. The shear strength of ice-filled joints linearly increases with increasing the aggregation area of rupture ice before noticeable bulges. However, the relationship between the JRC index and the shear strength is not significant.

(3) The shear strength of ice-filled joints decreases with increasing joint opening. When the joint opening increases from 2 mm to 14 mm, the aggregation of rupture ice gradually disappears and the shear strength of ice-filled joint is equal to that of solid ice. A critical value of infilled thickness may exist, which need further study.

(4) The shear strength of ice-filled joints decreases when the shear rate increase from 0.2 mm/min to 0.8 mm/min. The infilled ice may change from ductile to brittle failure with increasing shear rate. The aggregation area of rupture ice also decreases while the brittle rupture phenomenon of joint ice is more obvious as the shear rate increases.

(5) The shear strength of ice-filled joints linearly increases with increasing normal stress, which well satisfies the Mohr-coulomb criterion. The aggregation area of rupture ice also increases with increasing normal stress. In addition, the improvement of shear strength caused by the normal stress is much larger for the ice-filled joints than the solid ice, because the bulges can prevent the lateral expansion of ice under compression.

516    **Acknowledgements**

517    This work was supported by National Natural Science Foundation of China (Grant No. 42072300 and

518    No. 41702291), Project of Natural Science Foundation of Hubei Province (Grant No. 2021CFA094).

519    **Conflict of interest**

520    The authors declared that they have no conflicts of interest to this work.

521    **Reference**

522    Allen, S. and Huggel, C.: Extremely warm temperatures as a potential cause of recent high mountain

523    rockfall, Global. Planet. Change., 107, 59-69, https://doi.org/10.1016/j.gloplacha.2013.04.007, 2013.

524    Barton, N. and Choubey, V.: The shear strength of rock joints in theory and practice, J. Rock. Mech.

525    Geotech., 10, 1-54,https://doi.org/10.1007/BF01261801, 1977.

526    Bragov, A., Igumnov, L., Konstantinov, A., Lomunov, A., Filippov, A., Shmotin, Y., Didenko R. and

527    Krundaeva, A.: Investigation of strength properties of freshwater ice, EPJ Web of Conferences., 94,

528    01070, https://doi.org/10.1051/epjconf/20159401070, 2015.

529    Colucci, R. R. and Guglielmin, M.: Climate change and rapid ice melt: Suggestions from abrupt

530    permafrost degradation and ice melting in an alpine ice cave, Prog. Phys. Geog., 43, 561-573,

531    https://doi.org/10.1177/0309133319846056, 2019.

532    Davies, M. C., Hamza, O. and Harris, C.: The effect of rise in mean annual temperature on the stability

533    of rock slopes containing ice-filled discontinuities, Permafrost. Periglac., 12, 137-144,

534    https://doi.org/10.1002/ppp.378, 2001.

535     Davies, M. C., Hamza, O., Lumsden, B. W. and Harris, C.: Laboratory measurement of the shear

536     strength of ice-filled rock joints, Ann. Glaciol., 31, 463-467,

537     https://doi.org/10.3189/172756400781819897, 2017.

538     Etzelmüller, B., Czekirda, J., Magnin, F., Duvillard, P. A., Ravanel, L., Malet, E., Aspaas A.,

539     Kristensen L., Skrede I., Majala G. D., Jacobs B., LeinauerJ., Hauck C., Hilbich C., Böhme M.,

540     Hermanns R., Eriksen H., Lauknes T. R., Krautblatter M. and Westermann, S.: Permafrost in monitored

541     unstable rock slopes in Norway–new insights from temperature and surface velocity measurements,

542     geophysical surveying, and ground temperature modelling, Earth. Surf. Dynam., 10, 97-129,

543     https://doi.org/10.5194/esurf-10-97-2022, 2022.

544     Fukuzawa, T. and Narita, H.: An experimental study on the mechanical behavior of a depth hoar layer

545     under shear stress. Ph.D. thesis, Institute of Low Temperature Science, Hokkaido University, Japan, 5 p

546     p., 1993.

547     Gruber, S. and Haeberli, W.: Permafrost in steep bedrock slopes and its temperature-related

548     destabilization following climate change, J. Geophys. Res.-Earth., 112, F02S18,

549     https://doi.org/10.1029/2006JF000547, 2007.

550     Han, H. W., Jia, Q., Huang, W. F. and Li, Z. J.: Flexural strength and effective modulus of large

551     columnar-grained freshwater ice, J. Cold. Reg. Eng., 30, 04015005,

552     https://doi.org/10.1061/(ASCE)CR.1943-5495.0000098, 2016.

553    Hartmeyer, I., Delleske, R., Keuschnig, M., Krautblatter, M., Lang, A., Schrott, L. and Otto, J. C.:

554    Current glacier recession causes significant rockfall increase: the immediate paraglacial response of

555    deglaciating cirque walls, Earth. Surf. Dynam., 8, 729-751, https://doi.org/10.5194/esurf-8-729-2020,

556    2020.

557    Hilger, P., Hermanns, R. L., Czekirda, J., Myhra, K. S., Gosse, J. C. and Etzelmüller, B.: Permafrost as

558    a first order control on long-term rock-slope deformation in (Sub-) Arctic Norway, Quaternary. Sci.

559    Rev., 251, 106718, https://doi.org/10.1016/j.quascirev.2020.106718, 2021.

560    Huang, S. B., Yu, S. L., Ye, Y. H, Ye, Z. Y. and Cheng, A. P.: Pore structure change and

561    physico-mechanical properties deterioration of sandstone suffering freeze-thaw actions, Constr. Build.

562    Mater., 330, 127200, https://doi.org/10.1016/j.conbuildmat.2022.127200, 2022.

563    Huang, S. B., Wang, J., Liu, Y. Z., Tian, Q. and Cai, C.: Experimental investigation on crack

564    coalescence and strength loss of rock-like materials containing two parallel water-filled flaws under

565    freeze-thaw. Theor. Appl. Fract. Mec., S0167-8442(22), 00413-X,

566    https://doi.org/10.1016/j.tafmec.2022.103669, 2022b.

567    Krautblatter, M., Funk, D., Günzel, F. K.: Why permafrost rocks become unstable: a

568    rock-ice-mechanical model in time and space, Earth. Surf. Proc. Land., 38, 876-887,

569    https://doi.org/10.1002/esp.3374, 2012.

570     Krautblatter, M., Huggel, C., Deline, P. and Hasler, A.: Research perspectives on unstable high-alpine

571     bedrock permafrost: Measurement, modelling and process understanding, Permafrost. Periglac., 23,

572     80-88, https://doi.org/10.1002/ppp.740, 2021.

573     Legay, A., Magnin, F. and Ravanel, L.: Rock temperature prior to failure: Analysis of 209 rockfall

574     events in the Mont Blanc massif (Western European Alps), Permafrost. Periglac., 32, 520-536,

575     https://doi.org/10.1002/ppp.2110, 2021.

576     Lou, X. N. and Wu, Y.: Influence of temperature and fiber content on direct shear properties of plain ic

577     e       and       fiber-reinforced       ice,       Cold.       Reg.       Sci.       Technol.,       194,       103458,

578     https://doi.org/10.1016/j.coldregions.2021.103458, 2021.

579     Luo, S., Li, C., Li, F., Wang, J. and Li, Z. G.: Ice crystallization in shear flows, J. Phys. Chem. C., 123,

580     21042-21049, https://doi.org/10.1021/acs.jpcc.9b06225, 2019.

581     Mamot, P., Weber, S., Eppinger, S. and Krautblatter, M.: A temperature-dependent mechanical model

582     to assess the stability of degrading permafrost rock slopes, Earth. Surf. Dynam., 9, 1125-1151,

583     https://doi.org/10.5194/esurf-9-1125-2021, 2021.

584     Mamot, P., Weber, S., Schröder, T. and Krautblatter, M.: A temperature-and stress-controlled failure

585     criterion       for       ice-filled       permafrost       rock       joints,       Cryosphere.,       12,       3333-3353,

586     https://doi.org/10.5194/tc-12-3333-2018, 2018.

587     Matsuoka, N. and Murton, J.: Frost weathering: recent advances and future directions, Permafrost.

588     Periglac., 19, 195-210, https://doi.org/10.1002/ppp. 620, 195-210.

589 Petrovic, J. J.: Review mechanical properties of ice and snow, J. Mater. Sci., 38, 1-6,

590 https://doi.org/10.1023/A:1021134128038, 2003.

591 Ren, X. H.: Investigation on ductile-to-brittle transition behavior of ice, Ph.D. dissertation, Dalian

592 University of Technology, China, 64 pp, 2005.

593 Schulson, E. M. and Fortt, A. L.: Friction of ice on ice, J. Geophys. Res.-Sol. Ea., 117, B12204,

594 https://doi.org/10.1029/2012JB009219, 2012.

595 Shan, R. L., Bai, Y., Ju, Y., Han, T. Y., Dou, H. Y. and Li, Z. L.: Study on the triaxial unloading creep

596 mechanical properties and damage constitutive model of red sandstone containing a single ice-filled

597 flaw, Rock. Mech. Rock. Eng., 54, 833-855, https://doi.org/10.1007/s00603-020-02274-1, 2021.

598 Shen, Y. J., Yang, H. W., Xi, J. M., Yang, Y., Wang, Y. Z. and Wei, X.: A novel shearing fracture

599 morphology method to assess the influence of freeze-thaw actions on concrete-granite interface, Cold.

600 Reg. Sci. Technol., 169, 102900, https://doi.org/10.1016/j.coldregions.2019.102900, 2020.

601 Shugar, D. H., Jacquemart, M., Shean, D., Bhushan, S., Upadhyay, K., Sattar, A., Schwanghart, W.,

602 Mcbride, S., Van Wyk De Vries, M., Mergili, M., Emmer, A., Deschamps-Berger, C., Mcdonnell, M.,

603 Bhambri, R., Allen, S., Berthier, E., Carrivick, J. L., Clague, J. J., Dokukin, M., Dunning, S. A., Frey,

604 H., Gascoin, S., Haritashya, U. K., Huggel, C., Kääb, A., Kargel, J. S., Kavanaugh, J. L., Lacroix, P.,

605 Petley, D., Rupper, S., Azam, M. F., Cook, S. J., Dimri, A. P., Eriksson, M., Farinotti, D., Fiddes, J.,

606 Gnyawali, K. R., Harrison, S., Jha, M., Koppes, M., Kumar, A., Leinss, S., Majeed, U., Mal, S., Muhuri,

607 A., Noetzli, J., Paul, F., Rashid, I., Sain, K., Steiner, J., Ugalde, F., Watson, C. S. and Westoby, M. J.:

608     A massive rock and ice avalanche caused the 2021 disaster at Chamoli, Indian Himalaya, Science., 373,

609     300-306, 10.1126/science.abh4455, 2021.

610     Sinha, N. K.: Elasticity of natural types of polycrystalline ice, Cold. Reg. Sci. Technol., 17, 127-135,

611     https://doi.org/10.1016/S0165-232X(89)80003-5, 1989.

612     Walter, F., Amann, F., Kos, A., Kenner, R., Phillips, M., de Preux, A., Huss, M., Tognacca, C., Clinton,

613     J., Diehl, T. and Bonanomi, Y.: Direct observations of a three million cubic meter rock-slope collapse

614     with almost immediate initiation of ensuing debris flows, Geomorphology., 351, 106933,

615     https://doi.org/10.1016/j.geomorph.2019.106933, 2019.

616     Wang, C., Li, Y., Dai, F., Wu, G. N., Yin, F. T., Li, K. P. and Wang, K.: Experimental investigation on

617     mechanical properties and failure mechanism of rock-like specimens containing an arc-shaped ice-fille

618     d flaw under uniaxial compression, Theor. Appl. Fract. Mec., 119, 103368,

619     https://doi.org/10.1016/j.tafmec.2022.103368, 2022.

620     Weber, S., Fäh, D., Beutel, J., Faillettaz, J., Gruber, S. and Vieli, A.: Ambient seismic vibrations in

621     steep bedrock permafrost used to infer variations of ice-fill in fractures, Earth. Planet. Sc. Lett., 501,

622     119-127, https://doi.org/10.1016/j.epsl.2018.08.042, 2018.

623     Yang, Q. Q., Su, Z. M., Cheng, Q. G., Ren, Y. H. and Cai, F.: High mobility of rock-ice avalanches:

624     Insights from small flume tests of gravel-ice mixtures, Eng. Geol., 260, 105260,

625     https://doi.org/10.1016/j.enggeo.2019.105260, 2019.

626 Xu, D. P., Feng, X. T., Cui, Y. J.: A simple shear strength model for interlayer shear weakness

627 zone. Eng. Geol., 147, 114-123, http://dx.doi.org/10.1016/j.enggeo.2012.07.016, 2012.

628 Zhang, G. Z., Chen, G. Q., Xu, Z. X., Yang, Y. and Lin, Z. H.: Crack failure characteristics of different

629 rocks under the action of frost heaving of fissure water, Front. Earth. Sc.-Switz., 8, 13,

630 https://doi.org/10.3389/feart.2020.00013, 2020.

631 Zhao, Y. L., Zhang, L. Y., Asce, F., Wang, W. J., Liu, Q., Tang, L. M. and Cheng, G. M.: Experimental

632 Study on Shear Behavior and a Revised Shear Strength Model for Infilled Rock Joints, Int. J. Geomech.,

633 20(9), 04020141, 10.1061/(ASCE)GM.1943-5622.0001781, 2020.

634 Zhao, Z. H., Yang, J., Zhou, D. and Chen, Y. F.: Experimental investigation on the wetting-induced

635 weakening of sandstone joints, Eng. Geol., 225, 61-67, https://doi.org/10.1016/j.enggeo.2017.04.008,

636 2017.